Patterns of spontaneous motility in videomicrographs of human epidermal keratinocytes (HEK)

Wolfgang Alt, Oana Brosteanu, Boris Hinz, and Hans Wilhelm Kaiser

Abstract: The subject of our observations was the spontaneous behaviour of normal and transfected human epidermal keratinocytes. Cell movements were recorded on video micrographs and analyzed by a mathematical approach, using new methods of image processing and statistical correlation analysis. Protrusive activity of single lamellae was examined using one-dimensional analysis of phase-contrast image sequences along section lines transversal to the cell edge. This method revealed high periodicity and correlation in the motility patterns of lamellae and ruffles. Two-dimensional correlation analysis of automatically digitized cell outlines was applied to detect spatiotemporal patterns and coordination of lamellar extension and retraction. Most cells showed regularly alternating pulsations of lamellar protrusions. In some extreme cases, extension waves rotating around the cell periphery were observed. The results were compared with computer simulations of two simple models for lamellar dynamics and shape deformation, based on few assumptions about chemical kinetics of F-actin and cytomechanical properties of the actin network, neglecting regulatory effects of actin-associated proteins or extracellular stimulations. The simulation results reproduced the main dynamical features of the observed real cells, indicating the possibility that the basic universal mechanism for lateral coordination of lamellipodial protrusion is the interplay between hydrostatic pressure and viscoeontractile tension in the cortical F-actin – plasma membrane complex.

Key words: keratinocytes, cytomechanics, actin network, statistical correlation analysis, mathematical models.

Résumé : Nous avons étudié le comportement spontané de kératinocytes épidermiques humains normaux ou transfectés. Les mouvements des cellules ont été enregistrés sur des vidéomicrographies et analysés par une approche mathématique en utilisant de nouvelles méthodes de traitement d'image et d'analyse de corrélation statistique. La protrusion de lamelles individuelles a été étudiée par une analyse unidimensionnelle de séquences d'images en contraste de phase prises en coupe transversale le long du bord des cellules. Cette méthode a mis en évidence une périodicité et une corrélation importantes des motifs de déplacement des lamelles et des rides. Une analyse de corrélation bidimensionnelle des contours cellulaires numérisés automatiquement a été effectuée pour détecter les motifs spatio-temporels et la coordination de l'extension et de la rétraction des lamelles. La plupart des cellules ont des pulsations de protrusions de lamelles qui alternent régulièrement. Dans des cas extrêmes, des ondes d'extension se déplaçant autour de la périphérie des cellules sont observées. Ces résultats sont comparés à ceux des simulations par ordinateur effectuées avec deux modèles simples de la dynamique et du changement de forme des lamelles, en se basant sur quelques hypothèses concernant la cinétique chimique de l'actine F et les propriétés cytomécaniques du réseau d'actine, en négligeant la régulation exercée par les protéines associées à l'actine ou les stimulations extracellulaires. Les résultats des simulations reproduisent les caractéristiques dynamiques principales notées lors de l'observation réelle des cellules. Donc, le mécanisme fondamental universel de coordination latérale de la protrusion des lamellipodes pourrait être attribuable à l'interaction de la pression hydrostatique et de la tension visco-contractile du complexe entre l'actine F corticale et la membrane plasmique.

Mots clés : kératinocytes, cytomécanique, réseau d'actine, analyse de corrélation statistique, modèles mathématiques.

[Traduit par la rédaction]

Received March 14, 1995. Accepted August 1, 1995.

Abbreviations: HEK, human epidermal keratinocyte; trHEK, transformed HEK; nHEK, normal HEK; TBS, Tris-buffered saline; Tris, tris(hydroxymethyl)aminomethane; BSA, bovine serum albumin; PHEM, PIPES–HEPES–EGTA–$MgCl_2$; PIPES, 1,4-piperazinediethanesulfonic acid; HEPES, *N*-[2-hydroxyethyl]piperazine-*N*′-2-ethylsulfonic acid; EGTA, ethylene glycol bis(β-aminoethyl ether)-*N*,*N*-tetraacetic acid.

W. Alt,[1] **O. Brosteanu, and B. Hinz.** Division of Theoretical Biology, University Bonn, Kirschallee 1-3, D-53115, Bonn, Germany.
H.W. Kaiser. Department of Dermatology, University Bonn, Sigmund-Freud Str. 25, D-53127, Bonn, Germany.

[1] Author to whom all correspondence should be addressed.

Fig. 1. Representative distribution of F-actin in (A) nHEK and (B) trHEK. F-actin was demonstrated by application of rhodamine–phalloidine to permeabilized cultured keratinocytes grown in low calcium medium. Actin filaments appear in different structures, the two extreme cases being (*i*) evenly dispersed beneath the plasma membrane (this is obvious in the lamellar region) and more intensively dispersed at the border of the cell body as a result of superimposing of adjacent cortex (arrows in A; comparable with the halo in the phase-contrast image of Fig. 3A) and (*ii*) in regions of stress fibers, where actin filaments are aligned to bundles (arrowheads).

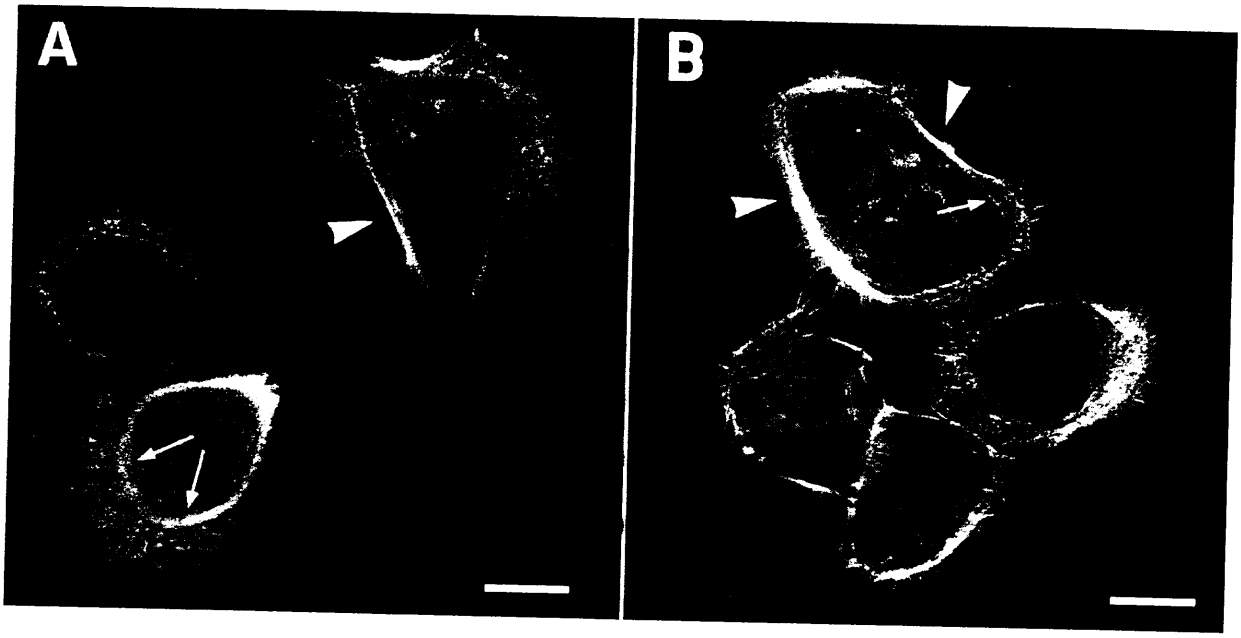

Introduction

Keratinocytes are located in the outer layer of the mammalian skin defined as epidermis, where they form a multilayer stratified epithelium. This epithelium generates itself by cell division of the basal keratinocytes, which are in close contact with the basal lamina. Subsequently, keratinocytes leave the basal lamina and finally differentiate into scales. In addition to vertical cell motion during differentiation, horizontal migration of keratinocytes is observed during wound healing. During this process, cells lose their contact with neighbouring cells and gain the ability to actively invade a wound (Donaldson and Mahan 1988). Apart from these benign conditions, keratinocyte migration is also observed during metastasis of squamous cell carcinoma.

Under culture conditions, where formation of cell–cell contacts is prevented, cells grow isolated (Figs. 1, 3A). A single motile keratinocyte, spread on a surface, consists of a cell body containing the main cytoplasm, nucleus, and cell organelles, surrounded by flat organelle-free extensions, called lamellae, giving the cell an overall appearance of a fried egg. In this initial situation, after spreading, the lamellar seam surrounds the whole cell body (Fig. 1A, cell in upper left), comparable with the analogous behaviour of Xenopus tadpole epidermal cells (Bereiter-Hahn and Lüers 1994). In the case of continuous migration, the cell polarizes and forms a dominant leading lamella (Fig. 1A, cell in lower left) but usually smaller than the one observed for fast-moving fish keratocytes (Lee et al. 1993). When stationary, the cell shows varying protrusive activity at the cell edge with regions of extended lamellar seam (Fig. 3A, *l*) and regions of stretched cell border without lamellae (Fig. 1, arrowheads; Fig. 3A, *st*). In both cases, outward cell motion manifests preferentially at the tips of lamellae, where several small protrusions occur. Filopodia extend as thin spikes at the cell edges, being about 0.1 μm wide and up to several micrometres long. Forming filopodia is one possibility for motile cells to acquire new territory, extending lamellipodia is another. These protrusions have characteristics similar to lamellae but extend even flatter on the substrate (Condeelis 1993), and are smaller and more irregular. Finally, motile cells might be distinguished from inactive cells by the appearance of ruffles (Abercrombie et al. 1970), which often originate from lamellipodia that lift up from substrate, fold backwards, and remain perpendicular to the surface of the advancing lamella (Fig. 2) (Felder and Elson 1990). They start their course at the extreme edge of the lamella, move centripetally like a wave towards the cell body, and finally disappear at the border between lamella and cell body.

Backward movement of ruffles and other visible particles (Harris and Dunn 1972; Dembo and Harris 1981; Forscher and Smith 1988; Fisher et al. 1988; Kucik et al. 1990; De Brabander et al. 1990; Grebeçki 1994) suggests the steady exertion of an intracellular traction force directed towards the cell body. Apparently this force either induces a complete retraction of the lamella or is balanced by cell–substrate adhesion sites on the ventral surface of the lamella (Schmidt et al. 1993). Translation of this force to an elastic substrate has been demonstrated and measured with fibroblasts (Harris et al. 1980) and fish keratocytes (Lee et al. 1994). Since the highly flexible lipid bilayer of the cell membrane is moving independently (Kucik et al. 1990), intracellular force exertion has to be transduced by the underlying cytoskeleton in the lamella, consisting of a more or less dense network of actin filaments. It can be visualized by immunofluorescent staining (Fig. 1) and is characterized by high turnover, including assembly from monomeric G-actin, coordinated disassembly, and

Fig. 2. Organization of the microfilament system of cultured epidermal keratinocytes. Cells grown in low calcium medium were permeabilized with 0.75% Triton X-100 stabilizing filaments selectively at the same time with 5 μM phalloidine. F-actin was demonstrated by application of 5 μM skeletal muscle myosin S1, seen as little nodes at the filament strands (e.g., arrowhead in B). (A) an overview of a trHEK exhibiting regions of coordinated filament elevations at the cell margin. (B) One of the regions at the extreme cell edge in A is presented at higher magnification. (C) A small group of connected actin filaments elevated perpendicular to the orientation of the underlying filament system at the cell periphery. Position and size of this structure at the cell surface resemble ruffles seen in phase-contrast and scanning electron microscopy images of nonpermeabilized cells (not shown).

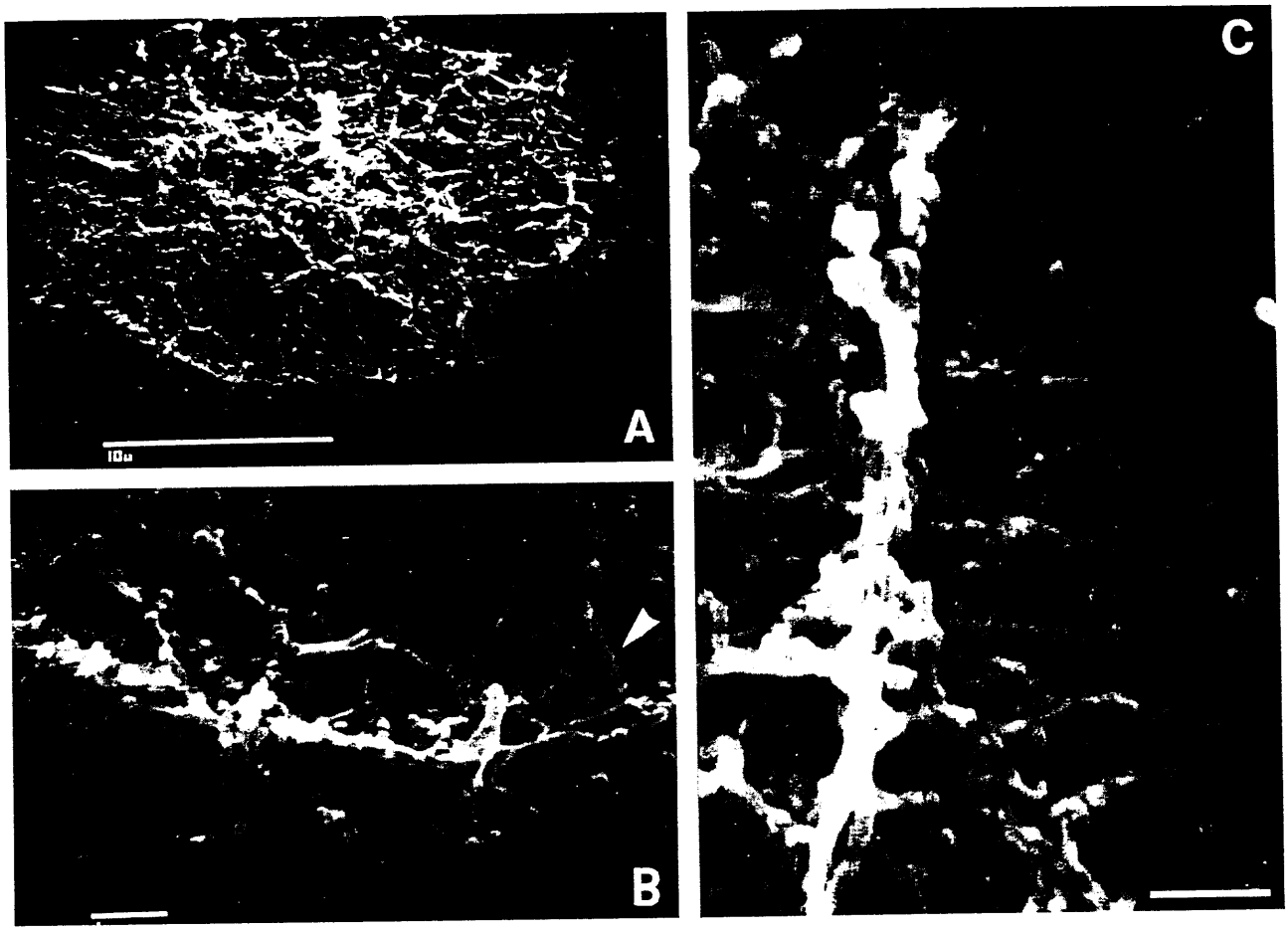

dynamic rearrangement of the actin network (Wang 1985; Cooper 1991; Theriot and Mitchison 1991). Blocking of actin polymerization by cytochalasin B inhibits forward cell movement, while the actin network is still retracted from the cell margin (Forscher and Smith 1988). Thus, assembly of actin filaments takes place preferentially at the tip, from where they are transported to the base of the lamella, apparently being already disassembled on their way (Symons and Mitchison 1991). Disassembly of acting filaments is supported by the presence of proteins like gelsolin (Weeds and Maciver 1993), and reorganization of the acting meshwork is facilitated by proteins like prolifin (Pring et al. 1992; Giuliano and Taylor 1994), thymosin (Machmias 1993), and gel-forming proteins like filamin (Hartwing and Kwiatkowski 1991). These actin-binding proteins are able to determine filament length and density of the network by severing, capping monomer-sequestering and crosslinking F-actin (Stossel 1993; Zigmond 1993; Giuliano and Taylor 1995). In addition, interaction with myosin II generates the contractile force on acting filaments that enables their retrograde flow (Heath and Holifield 1991), and interaction with other filament systems, such as microtubules and intermediate filaments, influences the polarity of the network arrangement (Vasiliev 1991).

Although the basic molecular ingredients for cell motion have been characterized, their physiological regulation and mechanical dynamics are not well understood. During assembly, actin filaments, whose pointed ends are preferentially oriented towards the cell body, have to access their barbed ends at the lamellar tip for further polymerization of actin monomers. The mechanism whereby this is achieved is still under discussion. Transient changes in actin polymerization (Evans 1993; Skierczynski et al. 1994) and protrusion of the cell membrane due to local osmotic swelling at the lamellar tips have been discussed (Condeelis et al. 1990; Bray et al. 1991). Brownian movement of the cell membrane (Peskin et al. 1993) and the action of myosin I detaching the membrane from the underlying filaments (Sheetz et al. 1992; Fath and Burgess 1994) have also been suggested. Finally, the role of hydrostatic pressure and mechanical tension for local dynamics and microfilament alignment has also been mentioned (Kolega 1986; Korohoda et al. 1992; Bray and White 1988). However, mechanisms inducing global coordination of cell movements

have received little attention. Retraction of one lamella is often accompanied by the appearance of a new lamella at a different site of the cell edge.

In the current study, we want to contribute to a solution to these questions by focussing on spontaneous cell movement of normal keratinocytes as well as keratinocytes transformed by the E6/E7 oncogene of HPV18 virus. Cell movements were recorded on video micrographs and analyzed by a mathematical approach using new methods of image processing and statistical correlation analysis, partly related to earlier studies with fibroblasts (Dunn and Brown 1990) or Dictyostelium (Killich et al. 1993, 1994). The results are compared with computer simulations of two simple models for lamellar dynamics (Alt 1990) and shape deformation (Alt and Tranquillo 1995), offering cytomechanical explanations for cell movement and thereby extending former proposals by Dembo et al. (1984), Oster et al. (1982), Oster (1984), Oster and Perelson (1987), Evans (1993), Luby-Phelps (1994), and Skierczynski et al. (1994).

Materials and methods

Cell culture

Cultures of human epidermal keratinocytes (nHEK) were obtained from newborn foreskins and initiated into culture by modification of a method developed by Rheinwald (1975) and Green et al. (1979). Subcultures were grown in MCDB 153 with 0.03 mM Ca^{2+}. Medium was supplemented with bovine pituitary extract (240 μg/mL), epidermal growth factor (0.1 ng/mL), ethanolamine (0.1 mM), insulin (750 μg/mL), penicillin (100 U/mL), phosphoethanolamine (0.1 mM), streptomycin (100 U/mL), and supplementary essential amino acids (glutamine, 4 mM; histidine, 240 μM; methionine, 90 μM; phenylalanine, 90 μM; tryptophane, 45 μM; and tyrosine, 75 μM). Cells were generally used from passages 3–5. Transformed keratinocytes (trHEK) were sustained by transfection of human epidermal cell by genes E6/E7 of human papilloma virus type 18 (Barbosa and Schlegel 1989) and subcultured as described for nHEK.

Immunofluorescence

Cultured keratinocytes were grown on cover slips for 18 h, fixed in 2% formaldehyde for 5 min, and permeabilized with 0.2% Triton X-100 in TBS ($CaCl_2$, 1 mM; NaCl, 0.8%; Tris, 20 mM), pH 7.4, containing 0.1 mM Ca^{2+}. Rhodamine-conjugated phalloidine (Sigma Chemical Co.) was applied for 1 h at 25°C diluted 1:3000 (v/v) in TBS with 0.1 mM Ca^{2+} and 1% BSA. Cells were then washed in the same buffer without BSA three times for 5 min and mounted in 40% glycerol. Cells were examined with a Zeiss Axiophot microscope equipped with epifluorescence and photographed with Kodak Tri-X pan films processed in Ultrafin SF (Tetenal, Norderstedt, Germany) at 400 ASA.

Scanning electron microscopy

Keratinocytes were plated at 5000 cells/cm^2 and grown on round plastic cover slips (Sarstedt, Nürnbrecht, Germany) for 18 h. Cells were permeabilized with PHEM (PIPES, 60 mM; HEPES, 25 mM; $MgCl_2$, 2 mM; EGTA, 10 mM), pH 7.4, containing 5 μM phalloidin, 0.8% Triton X-100, 0.1 mM pepstatin, and 42 nM leupeptin for 2 min at 25°C according to methods adapted from Hartwig (1992). Microfilaments were demonstrated by treating extracted cells with 5 μM skeletal muscle myosin S1 in PHEM for 10 min at 25°C and then washing with PHEM. Cells were fixed with a solution of 0.2% tannic acid, 1% glutaraldehyde, and 10 mM sodium phosphate buffer, pH 7.5, for 10 min at 25°C followed by extensive washing with distilled water. Specimens were rapidly frozen in liquid nitrogen, freeze-dried for 2 days in a freeze drier, and coated with gold and carbon in a sputter coater (Edwards sputter coater 150 A and 150 B).

Time-lapse video microscopy

Video microscopy was performed using a 63 × 1.4 na phase planapochromat objective on an Axiovert 10 inverted microscope (Zeiss, Oberkochem, Germany), equipped with a video system containing a low-light video camera (AVT Horn BC-5 with control unit, Aalen, Germany) and a time-lapse video cassette recorder (Panasonic AG 6720 A). Prints of phase-contrast images were produced by a videocopy processor (Mitsubishi P68E) on thermal paper. Cells were seeded at 5000 cells/cm^2 in the observation chamber of an ad hoc constructed medium perfusion system. The chamber was perfused by prewarmed MCDB 153 with supplements at 0.1 mL/min. This flow velocity does not affect cell behaviour but guarantees a constant environment as well as ideal culture conditions for cells during long-term recording. Temperature was held at 31°C with a heating system (Lincom CO 60, Raczek Analysentechnik, Wedemark, Germany) placed on top of the chamber and controlled by an external temperature sensor (Testo 701, Testoterm, Lenzkirch, Germany). Long-term sequences (up to 10 h) of motile keratinocytes were recorded with a time-lapse factor of 8.0.

Analysis of membrane ruffles, lamellipodia, and filopodia

In a first approach to quantify the typical behaviour of membrane ruffles, short-term sequences of 15 min were taken from motile HEK at 26°C, 30°C, 34°C, and 38°C, respectively. To provide high precision in medium temperature, the chamber was not perfused in this experiment. Cells (10 per observation chamber) were recorded for each temperature value at an additional magnification of 1.6 with a time-lapse factor of 4.6.

One-dimensional statistics of dynamics along a section line

Resulting sequences were analyzed by computer-assisted methods using an image processor (BioScan OPTIMAS® version 3.01, 1991). A digital section line of defined length was laid over the keratinocyte image, perpendicular to the cell edge, extending from substrate outside the cell over the region of membrane ruffling into the main cell body. Every second (4.6 real time), the luminance profile (256 levels of gray with minimum value 0 ≡ black and maximum value 255 ≡ white) of structures along the line was recorded and saved (Figs. 3A, 3B). The resulting liminance data sets were plotted over time in a three-dimensional diagram (Fig. 3C). In phase-contrast images, ruffles manifest as dark thin structures appearing at the cell edge, exhibiting a constant centripetal movement and disappearing at the border of the cell body. To detect these dark structures selectively and for quantitative analysis of ruffle behaviour, a different diagram was more suitable (Fig. 3D). Luminance values below a given threshold were represented by topographic lines in a two-dimensional graph. The thresh-

Fig. 3. From digitized keratinocyte images to plots of luminance levels along a section line. (A) Typical phase-contrast videograph of a keratinocyte (nHEK) is reproduced showing characteristic dynamic structures: cb, cell body; fil, filopodia; l, lamella; lam, lamellipodia; ruf, ruffles; sl, section line; st, stretched cell border. Bar, 10 μm. (B) The luminance profile of structures along a section line perpendicular to the cell edge from the substrate ($x = 0$) into the cell body ($x = 64$) was digitally stored. (C) Luminance profiles over one section line of an nHEK were recorded at 34°C over 6 min by taking data sets every second (4.6 s real time). In a three-dimensional plot of such data sets over time, dark structures appear as valleys ("black" = luminance 0). Ruffles (see Fig. 3B) are characterized by low luminance values and constant movement, starting at the cell edge. The level lines of luminance values are drawn below a certain threshold (dark line in Fig. 3C), resulting in a two-dimensional topographic plot (Fig. 3D). In this diagram, ruffle dynamics become more clear in synopsis with lamellipodial dynamics. Position of cell edge over time (See Fig. 3B) is marked as a continuous line (arrows in Fig. 3D).

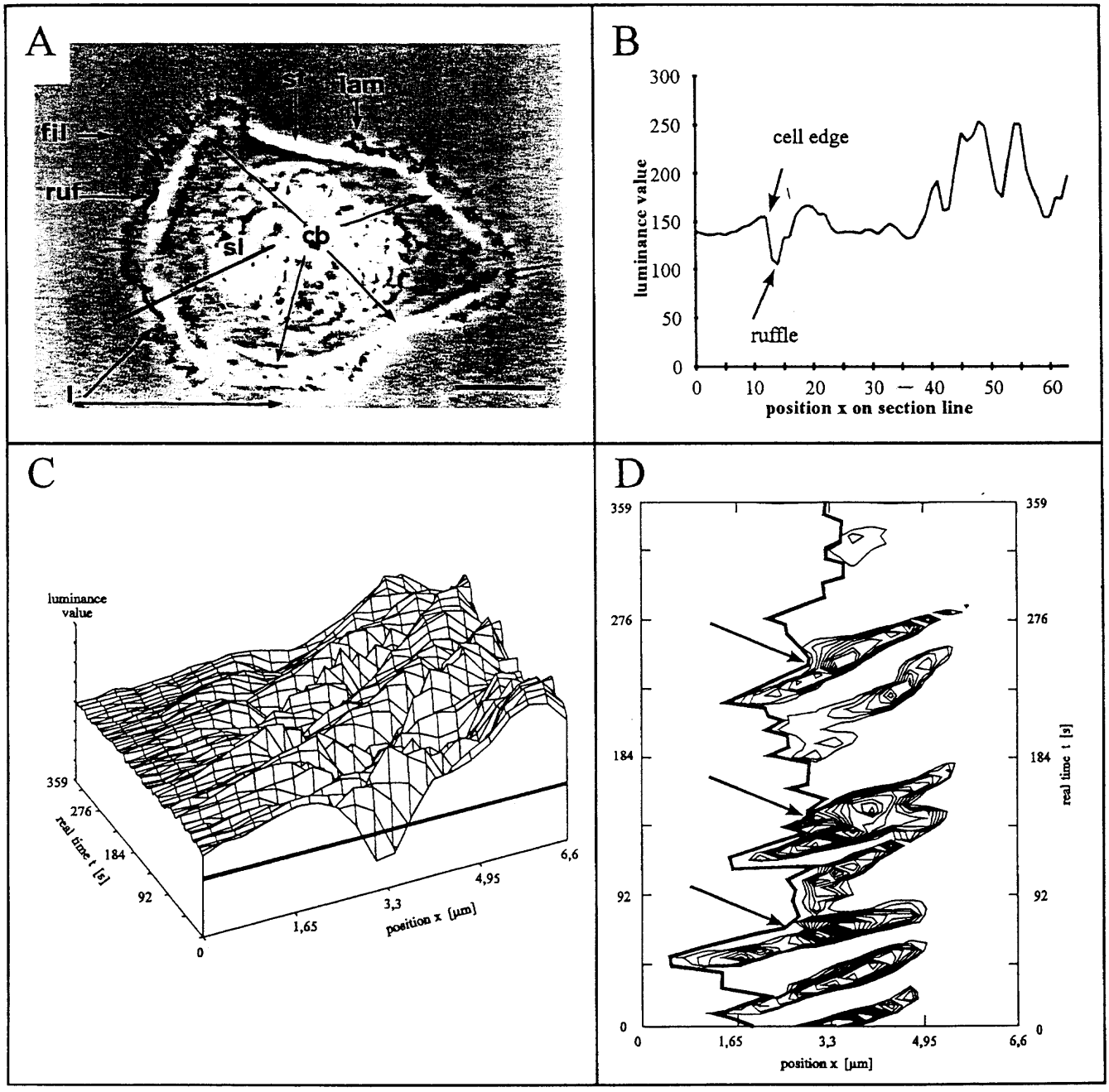

old was always set as five (relative) luminance values below the calculated mean background luminance. Variation of the threshold in a small range had only neglectable effect on the number of topographic lines but not on position and course of visible dark structures. Since ruffles show a constant time course, they are easily distinguished from more stationary internal phase-dense cell structures. Velocity of each appearing ruffle was measured graphically on diagram printouts of five regions per cell leading to 50 values per temperature. Dependence of ruffle velocity on temperature was assessed

using linear regression (Fig. 5A). Short-term sequences of 15 min were also used to determine velocities of lamellipodia and filopodia at four temperature values (Figs. 5B, 5C). Extension per minute of these structures was measured directly on video screen and, additionally, in the case of lamellipodia, by applying an edge detection algorithm to the data sets as in Fig. 3B. Temporal changes in position of the cell edge were depicted simultaneously with ruffle data in topographic plots (Fig. 3D), from which velocity of lamellipodia was determined as described above for ruffles. The newly developed edge detection algorithm is based on the assumption that the cell edge is marked by a (mostly sharp) transition between a bright halo surrounding the cell and darker intracellular structures represented by a (mostly steep) negative luminance gradient as in Fig. 3B. Using information on cell edge location in the preceding data set, $\tilde{x}$, the searching algorithm is constructed as a stochastic process around $\tilde{x}$, moving with positive searching velocity, ν, towards the cell body but being rejected by a decreasing luminance gradient: $\tau(X)$ is defined as luminance difference between X and the next following luminance minimum if luminance is decreasing and as 0 if luminance is increasing. More precisely, the process is a discretized solution of the stochastic differential equation

$$[1]\quad dX_s = (\nu - \alpha\cdot\tau(X_s) + \gamma\cdot\mathrm{sgn}(X_s - \tilde{x}) \cdot (X_s - \tilde{x})^2)\, ds + \sqrt{\beta}\, dW_s$$

with initial condition $X_{s=0} = 0$ (starting always outside the cell). Here s denotes the searching time and W_s is the standard Wiener process modeling white noise. The parameters ν, α, β, and γ are determined in dependence on contrast and resolution of the analyzed image. When the process X_s becomes stationary, the maximum $\{X\}_{max}$ is taken as the new cell edge position.

Periodicity of formation and movement of ruffles was examined on long-term video recordings. Thirty regions of 10 different cells with ruffle activity were observed for 60 min at 31°C as described above, and data sets of luminance values, $g(x, t)$ at position x on the section line at time, t, were entered into autocorrelation analysis. The autocorrelation was calculated with respect to an outstanding position $x = i$ on the section line that is passed by almost all occurring ruffles (Fig. 6A). Since ruffles manifest as dark structures relative to the mean luminance of the image, autocorrelation was calculated for the negative part of the normalized luminance data only. This allows the interpretation of positive values of the autocorrelation function as correlations between ruffles:

$$[2]\quad c_i(\alpha, \tau) = E_t([g(i,t) - E_t(g(i, \cdot))]_- \cdot [g(i + \alpha, t + \tau) - E_t(g(i + \alpha, \cdot))]_-)$$

where α is the correlation distance, τ is the correlation time, $E_t(\cdot)$ is the expectation value over time, t, and $[y]_- = \min\{y,0\}$ denotes the negative part of y.

Two-dimensional statistical correlation analysis of lamellar dynamics

Cell shape changes were analyzed using long-term video sequences of 15 nHEK and 15 trHEK. In periods of 3 s (24 s real time), video images of each sequence were digitized. Cell outlines were detected automatically and x- and y-coordinates of each pixel at the cell periphery were recorded using a new image processing program by Werner Heiβe (Theoretical Biology, University of Bonn, Bonn, Germany). Outlying points in the polygonal cell outline, occurring in regions with low phase contrast at the cell periphery, were removed using an algorithm based on calculation of the distance between neighbouring points. Subsequently, the contour line was smoothed. Because our objective was to analyze the spatiotemporal dynamics of the lamellar seam, i.e., the flat region surrounding a cell body, additional information on shape and location of the cell body was required. Because automatical recognition of cell body has not been developed yet, the border line of the cell body was manually digitized for the first video frame of the analyzed video sequence. For following data sets, location and shape of the cell body were simulated using information about the peripheral cell outline and the cell body as an inert cell region that changes shape and position only in reaction to global cell-shape changes or cell translocation.

Physical moments of the cell, up to second order, were estimated for every time, t, using different weights $f(x, y)$ for the bulky cell body and the flat lamellar seam. The assumption of a mass ratio of 20:1 between cell body and lamellar seam was used and the corresponding weighed momental ellipse was computed:

$$[3]\quad E_Z = [(x, y)^T | \mu_{02}x^2 - 2\mu_{11}xy + \mu_{20}y^2 = 4\mu_{20}\mu_{02} - 4\mu_{11}{}^2]$$

where μ_{20}, μ_{02}, and μ_{11} are the centralized second-order moments of the cell area, Z, around the centroid $S = (s_x, s_y)$:

$$[4]\quad \mu_{lk} = \int_Z (x - s_x)^l (y - s_y)^k f(x, y)\,dx\,dy \Big/ \int_Z f(x, y)\,dx\,dy,\ 0 \le l, k \le 2$$

This weighed momental ellipse has the same moments of second order as Z and approximates shape and orientation of the cell body. In Fig. 4, a cell outline is drawn together with the outline of the cell body and the calculated weighed momental ellipse. The cell outline was then, for every angle, φ, and observation time, t, represented as distance $z(\varphi, t)$ in normal direction between momental ellipse and cell outline (Fig. 4B). Finally, the three-dimensional data set of $z(\varphi, t)$ was printed as topographic level-line plot (Fig. 8). Protrusions are represented as elevated regions in the topographic plot, used to describe their spatiotemporal dynamics qualitatively, while quantitative analysis was provided by computing the autocorrelation function

$$[5]\quad c(\alpha, \tau) = E_{\varphi t}[(z(\varphi, t) - E_{\varphi t}(z(\varphi, t)))\cdot(z(\varphi + \alpha, t + \tau) - E_{\varphi t}(z(\varphi, t)))]$$

where $E_{\varphi t}(\cdot)$ is the expectation value over φ and t. Thus, $c(\alpha, \tau)$ is a measure for correlation of the cell outline in spatial distance $\alpha(0 \le \alpha < 2\pi)$ and temporal distance τ.

Models for lamellar dynamics

One-dimensional model for lamella protrusion–retraction and ruffle dynamics

To explain the observed forward (and backward) motion of

Fig. 4. Determination and presentation of normal extensions of the cell outline. (A) Final result of the automatic cell outline detection for one cell image is shown (outer line). The cell body was digitized manually from the first phase-contrast videograph of a sequence (inner line). The weighed momental ellipse approximating the cell body was calculated subsequently for every digitized picture at time, t. (B) Cell outline data were transformed into normal coordinates by calculating distances between ellipse and cell outline at 180 discrete angular positions (A, radii) and plotted as normal extensions $z(\varphi, t)$ over angle

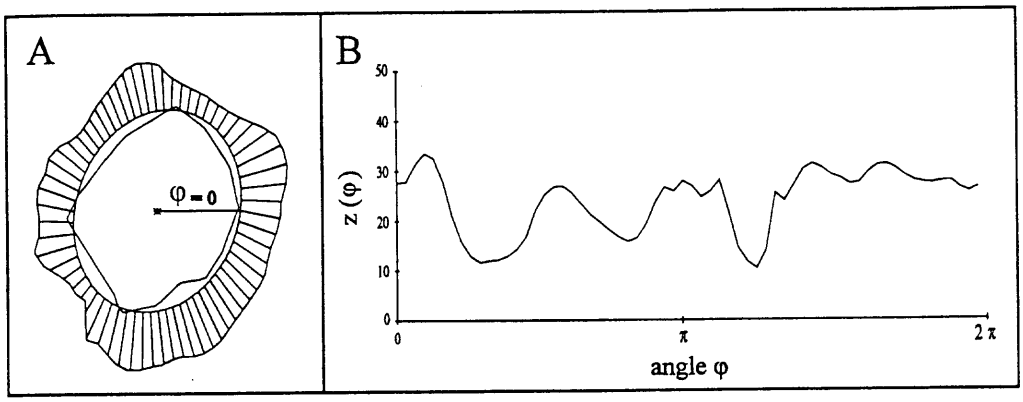

the lamellar tip as well as the formation and backward motion of ruffles along a section line (as in Fig. 3), we refer to a biochemical–mechanical model proposed by Alt (1990) and based on Dembo et al. (1984). The contractile actomyosin meshwork in the flat lamella is modelled as a highly viscous fluid, with a steady (negative) flow velocity $W = W(x, t)$ that draws newly assembled F-actin from the tip of the lamella, $x = L(t)$, back to the cell, $x = 0$. Assembly of F-actin at low and disassembly at high concentrations are reflected by the simple mass balance equation

$$[6] \quad \partial_t a + \partial_x(aW) = \eta(a_* - a)$$

for F-actin density, $a = a(x, t)$, $0 < x < L(t)$, with chemical equilibrium value a_*. Network viscosity, $\mu = \mu(a)$, is assumed to increase with a, whereas network tension, $\sigma(a) = \psi(a) + \sigma_0 \ln(1 - a/a_{max})$, is negative for low a because of solvation pressure (σ_0), but increases for larger a because of contractile interaction via myosin, $\psi(a)$, which for high values of a again decays as a result of compactification of the F-actin gel (see Alt 1990). At the tip, $x = L(t)$, the actin network might move inward

$$[7] \quad W(t, L(t)) \leq dL/dt = H\cdot(P_B - P_{base})$$

even while the tip is extending, $dL/dt > 0$. This happens if the hydrostatic pressure P_{base} from inside the lamella is less than the pressure P_B from the cell body, H denoting the hydraulic conductivity of the aqueous phase pouring through the dense cortical layer around the cell body. The hydrostatic pressure drops from P_{base} at the base to P_{tip} at the tip of the lamella, proportional to the total drag force onto the actin network:

$$[8] \quad P_{base} - P_{tip} = \Phi \int_0^{L(t)} a(x, t)(dL(t)/dt - W(x, t))\, dx$$

where Φ denotes the drag coefficient. Finally, we assume that the tip pressure, P_{tip}, equilibrates to

$$[9] \quad P_{tip} = \mu(a)\partial_x W + \sigma(a) + F_{tip}, \qquad \text{at } x = L(t)$$

i.e., the viscocontractile tension of the actin–myosin network plus an inward normal force F_{tip} exerted by the cortical actin–membrane complex onto the fluid in the lamella. In a full two- or three-dimensional model, F_{tip} would depend on cortical surface tension and curvature (equation 13); however, for the one-dimensional model, we assume a simple monotone increasing dependence on lamella length, L, and F-actin density, a, at the tip:

$$[10] \quad F_{tip} = (\gamma + \beta a)/\sqrt{1 + \kappa/L^4}$$

Equations 6–10 together with a force balance equation for network tension, *cp* (Alt 1990), constitute a well-posed dynamic system describing the "fluid mechanics" along a one-dimensional section through a lamella, neglecting any other impacts as substrate adhesion, two- or three-dimensional geometry, or inhomogeneities in density or supply of G-actin, myosin, or other actin-binding proteins.

Circular model for cortical cytomechanics and two-dimensional shape deformations

For describing spontaneous motility and shape deformations of keratinocytes spread on a surface with a more or less rounded periphery, as some cells in Fig. 1, we refer to a simplified cytomechanical differential equation system (Alt and Kaiser 1994; Alt and Tranquillo 1995). It models the peripheral actomyosin distribution $a = a(\varphi, t)$ over angular position φ of the lamella seam with varying radial extension $L = L(\varphi, t)$. The local mass of cortical F-actin, $L\cdot a$, might move along the periphery with tangential velocity $V = V(\varphi, t)$

$$[11] \quad \partial_t(La) + \partial_\varphi(La\cdot V) = L\cdot\eta(a_* - a)$$

as a result of the balance between contractile and viscous stresses as before, but now we consider only the tangential components and an additional compressive (dilative) stress resulting from cortical surface tension (τ) and a negative (positive) curvature of the cell outline $R(\varphi, t) = R_0 + L(\varphi, t)$

$$[12] \quad aV = \partial_\varphi(\mu a\partial_\varphi V + \sigma(a) - \partial_\varphi(\tau a\partial_\varphi L))$$

Fig. 5. (A) Retraction velocity of ruffles, (B) extension velocities of lamellipodia, and (C) filopodia of normal and transfected keratinocytes depending on temperature. Single values are represented by dots and linear regression values are represented by solid lines for nHEK and stippled lines for trHEK. Temperature dependence of all cell structures is almost linear between 26°C and 34°C and gets saturated at 38°C. (D) The adjusted linear regression coincide well with the experimental means (data not shown). Extension of filopodia is significantly faster than that of lamellipodia, with lamellipodial extension speed of trHEK exceeding that of nHEK, which in both cases is about twice the retraction speed of ruffles.

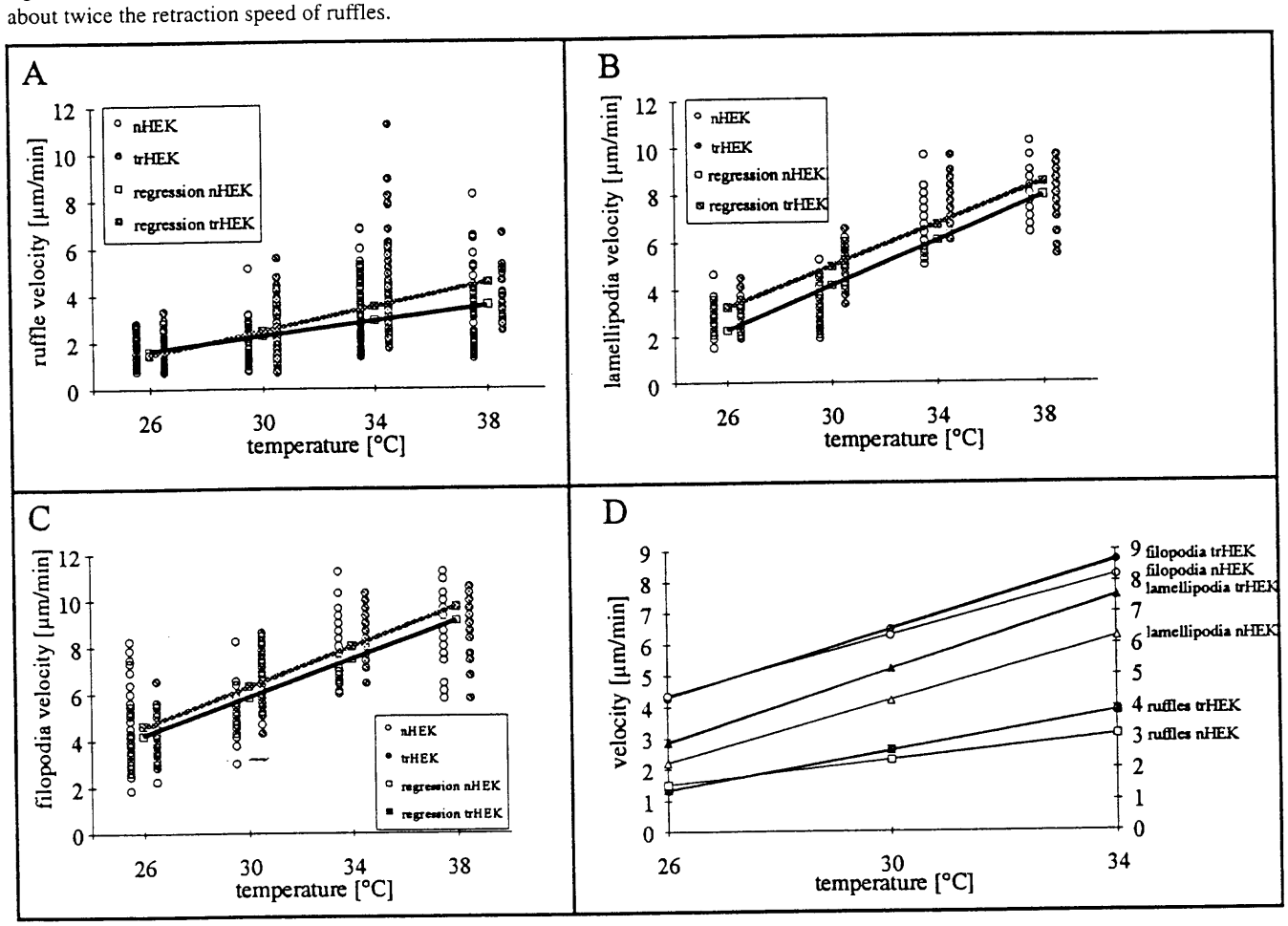

Table 1. Regression lines of velocity depending on temperature.

	Ruffles	Lamellipodia	Filopodia
nHEK	$-2.66 + 0.16 \cdot T$	$-10.18 + 0.48 \cdot T$	$-6.42 + 0.41 \cdot T$
trHEK	$-5.11 + 0.26 \cdot T$	$-8.14 + 0.44 \cdot T$	$-6.39 + 0.42 \cdot T$
	$p = 0.00001$	$p = 0.000005$	$p = 0.00019$

Table 2. Mixed linear model for velocity of ruffles, lamellipodia, and filopodia: influence of model parameters.

	Cell type	Temperature (T)	Individual cell	Cell type·T
Ruffles	$p = 0.011$	$p = 0.000$	$p = 0.000$	$p = 0.195$
Lamellipodia	$p = 0.000$	$p = 0.000$	$p = 0.000$	$p = 0.000$
Filopodia	$p = 0.012$	$p = 0.000$	$p = 0.000$	$p = 0.038$

Fig. 6. Long-term observation and autocorrelation analysis of ruffle dynamics. (A) Ruffle activity along a section line (see Fig. 3A, sl) in one cell region was recorded for 70 min at 31°C and a 45.5-min section was plotted as described for Fig. 3D. Topographic lines for luminance values below a given threshold were drawn over time t, and position x on the section line. An observation frame (light grey) with a reference line at position $x = i$ and width $2n + 1$ was determined. For correct calculation, it was important to include all ruffles in the observation frame being passed by the reference line at $x = i$. (B) Autocorrelation plot. Long data sets were entered into autocorrelation analysis (equation 2) to detect periodical patterns in ruffle movement at one cell region. Autocorrelation is referred to the reference line $x = i$ and was performed for correlation distances α in $[-n, n]$ (light grey) and for correlation times α in $[-\tau_{max}, \tau_{max}]$, including at least two subsequent ruffles completely. The resulting correlation frame (dark grey in A) was moved step by step over all ruffles, autocorrelation of underlying luminance values was calculated and again plotted as topographic lines in B. Highest correlation between two points, represented by the center of topographical line arrangements, stands for high probability of a second ruffle to form at distance α and correlation time τ over the whole observation period. Free areas represent none or negative autocorrelation to the reference point.

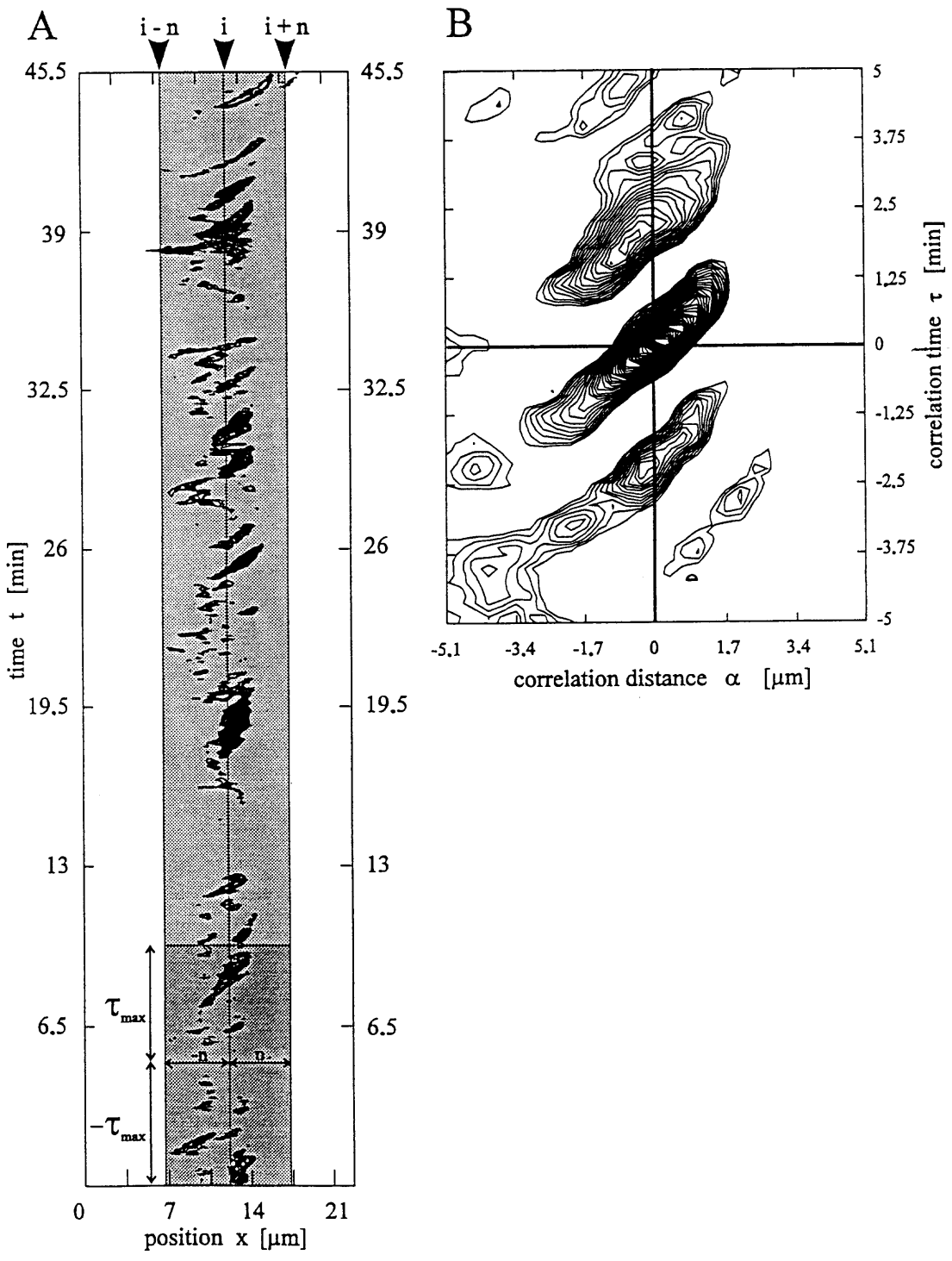

Fig. 7. Sequence of keratinocyte images over a period of 264 min printed in intervals of 24 min real time. The trHEK remains almost stationary with short periods of migration (A), but extends and retracts lamellae at three preferred regions (arrowheads in B). The cell outline was determined automatically by a two-dimensional edge detecting program and data were further processed to give a continuous cell circumference (B). The cell body is approximated by the weighed momental ellipse (broken line in B). Bar, 10 μm.

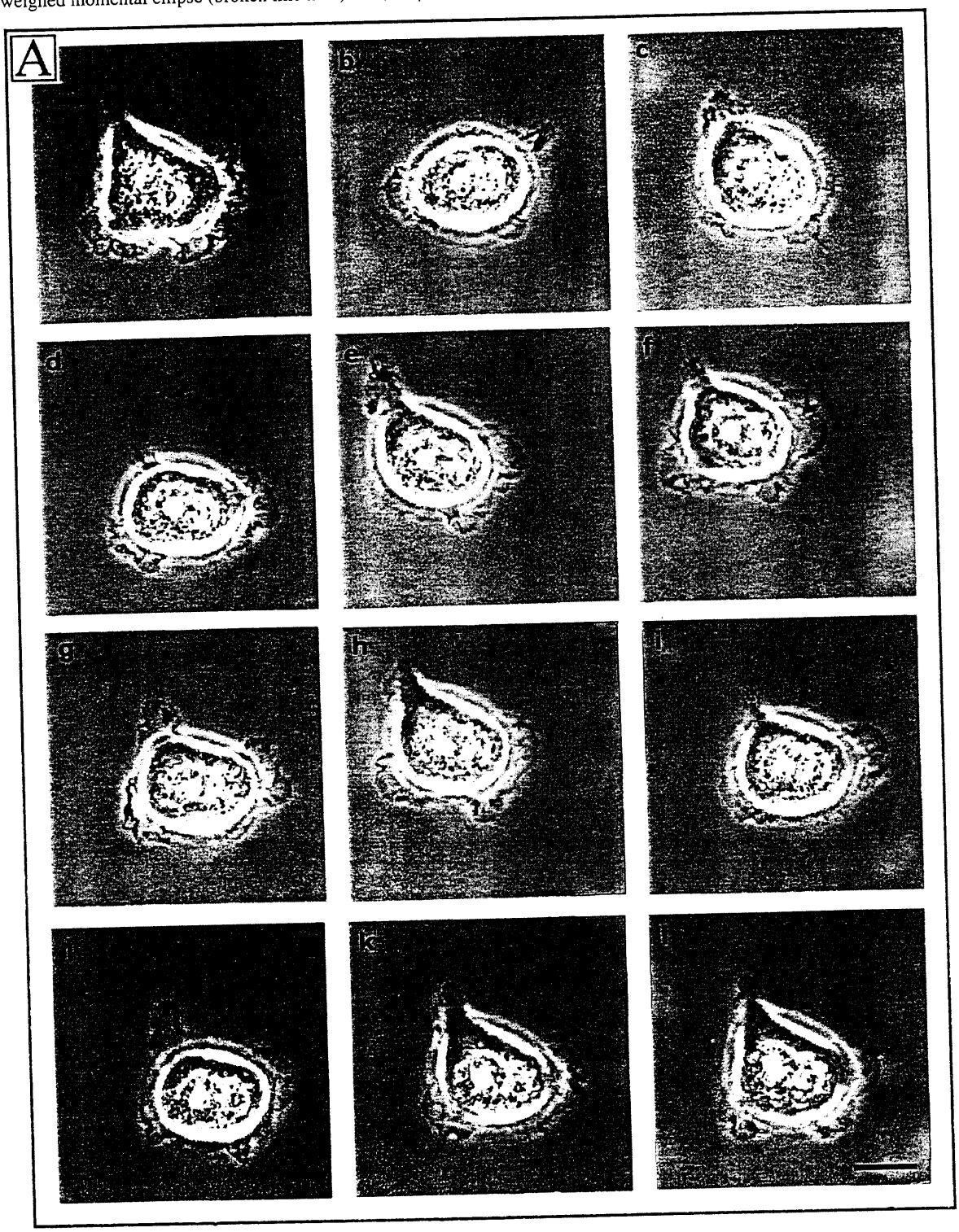

Fig. 7. (Concluded).

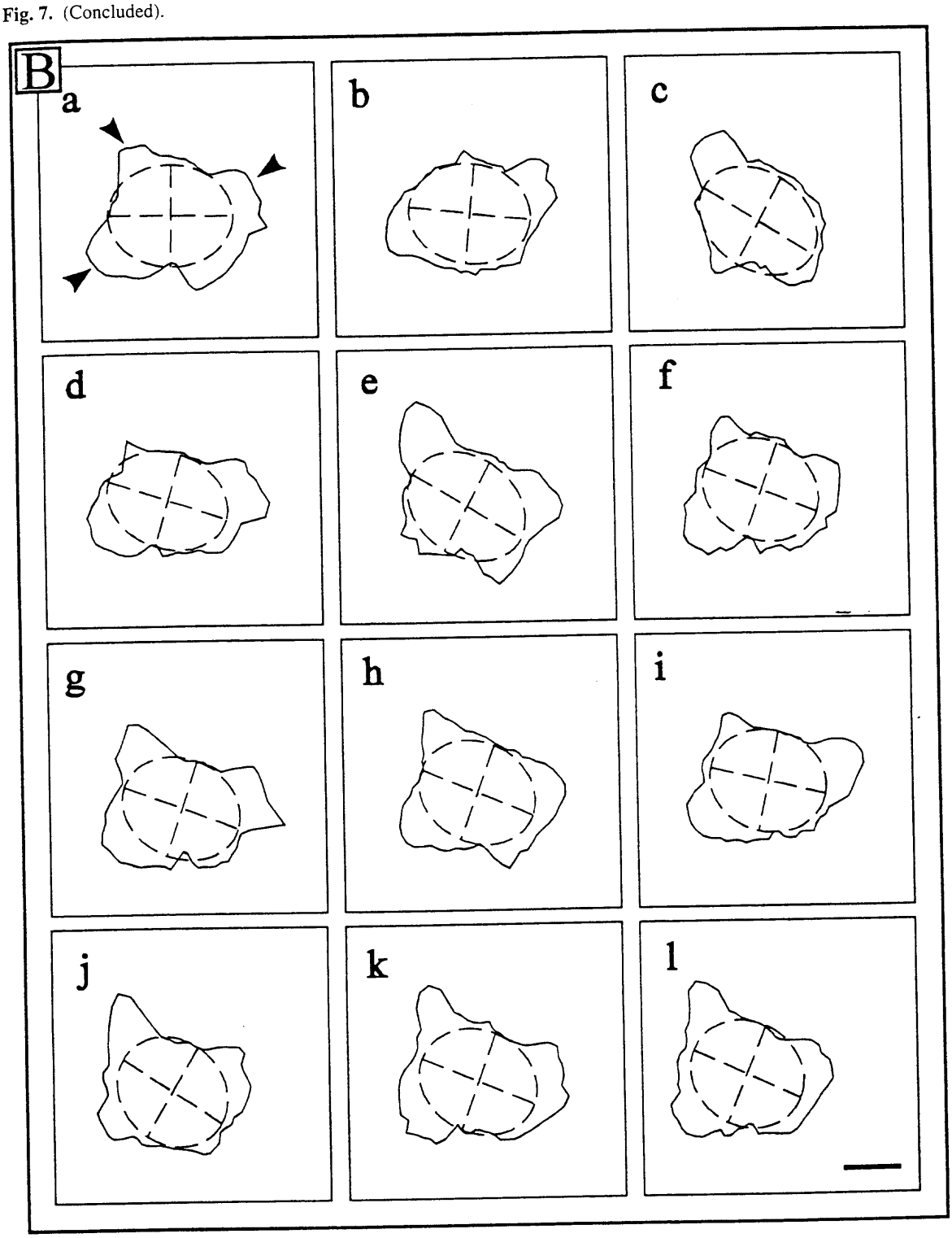

Fig. 8. Topographic plots of parametrized cell outlines of keratinocytes over angle, φ, and time, t. Lamellipodial dynamics of keratinocytes observed at 31°C were digitally computed as described for Fig. 4 and cell outline data $z(\varphi, t)$ were printed as topographic lines above the expectation value in analogy to Fig. 3D. (A) Lamella of nHEK were generally persistent over long time periods, Fig. 8A gives a representative example for all examined cells. Continuous retraction of one lamella (at $\pi/2$) was correlated to the extension of an antipodal new lamella (at $3/2\ \pi$), as it could be observed from 0 to 18 min and between 100 and 160 min. (B) Lamellar dynamics of trHEK-1 exhibited a clearly periodic pattern over time. The keratinocyte formed antipodal lamellae at $\pi/4$ and $5/4\pi$, alternating with high frequency. (C) Another cell, trHEK-2, showed no alternating behaviour of lamellae but exhibited only one lamella rotating in a counterclockwise direction around the cell periphery, with longer lasting and broader extension of the lamella in two regions (at π and 2π).

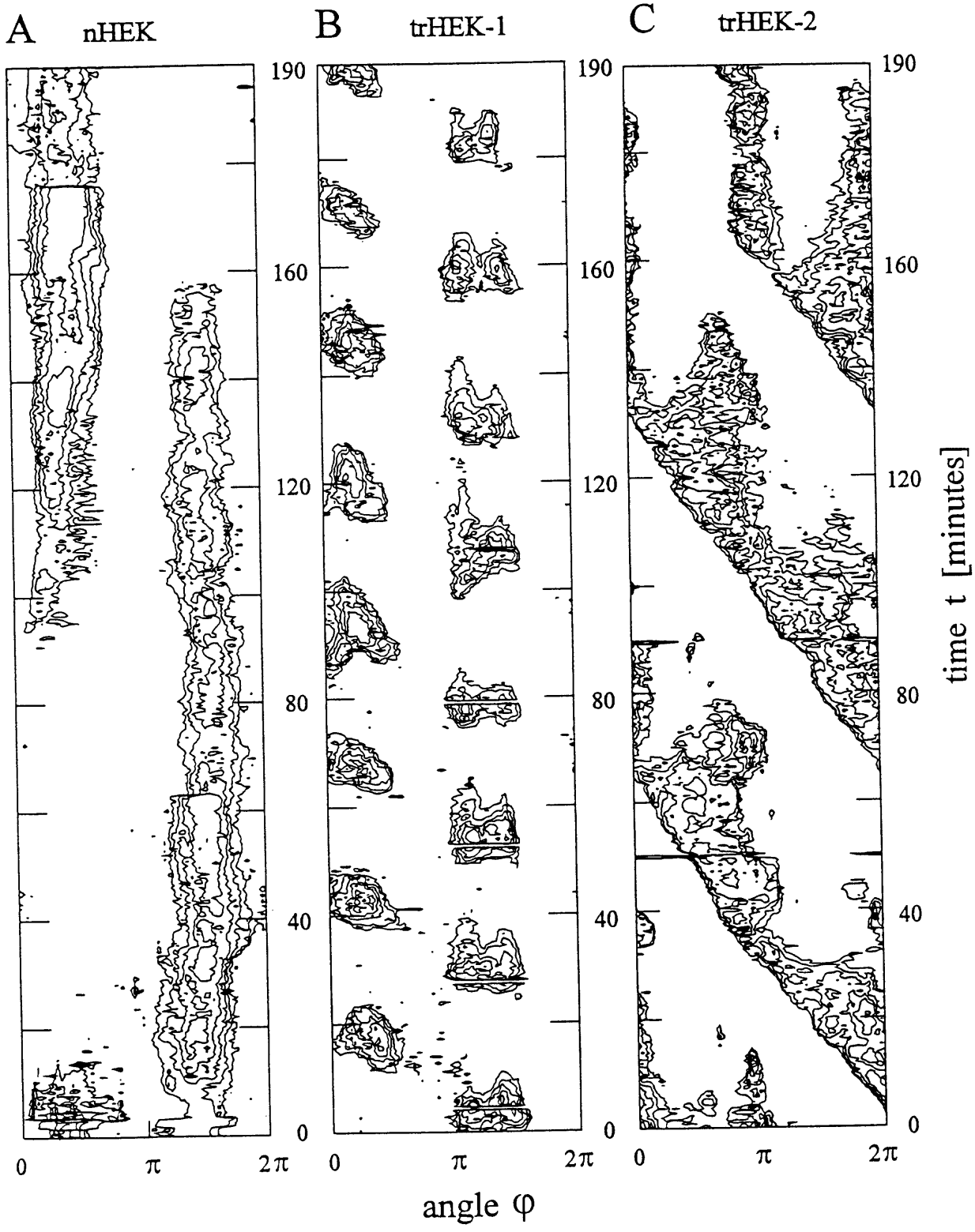

Fig. 9. Autocorrelation analysis of lamellar dynamics. (A, B, C) Autocorrelation results corresponding to the two-dimensional topographic plots in Fig. 6 are presented. Correlation values were plotted as three-dimensional diagrams over correlation time, τ, between 0 and 40 min and correlation angle, α, representing the mean (equation 5) behaviour of the cell periphery over the whole observation period of 190 min. High correlation values therefore symbolize high regularity in lamellar extension formed at a given time distance τ and a given angular distance α. (*a*, *b*, *c*) For quantitative analysis, two-dimensional topographic plots of correlation values above the expectation value 0 were printed.

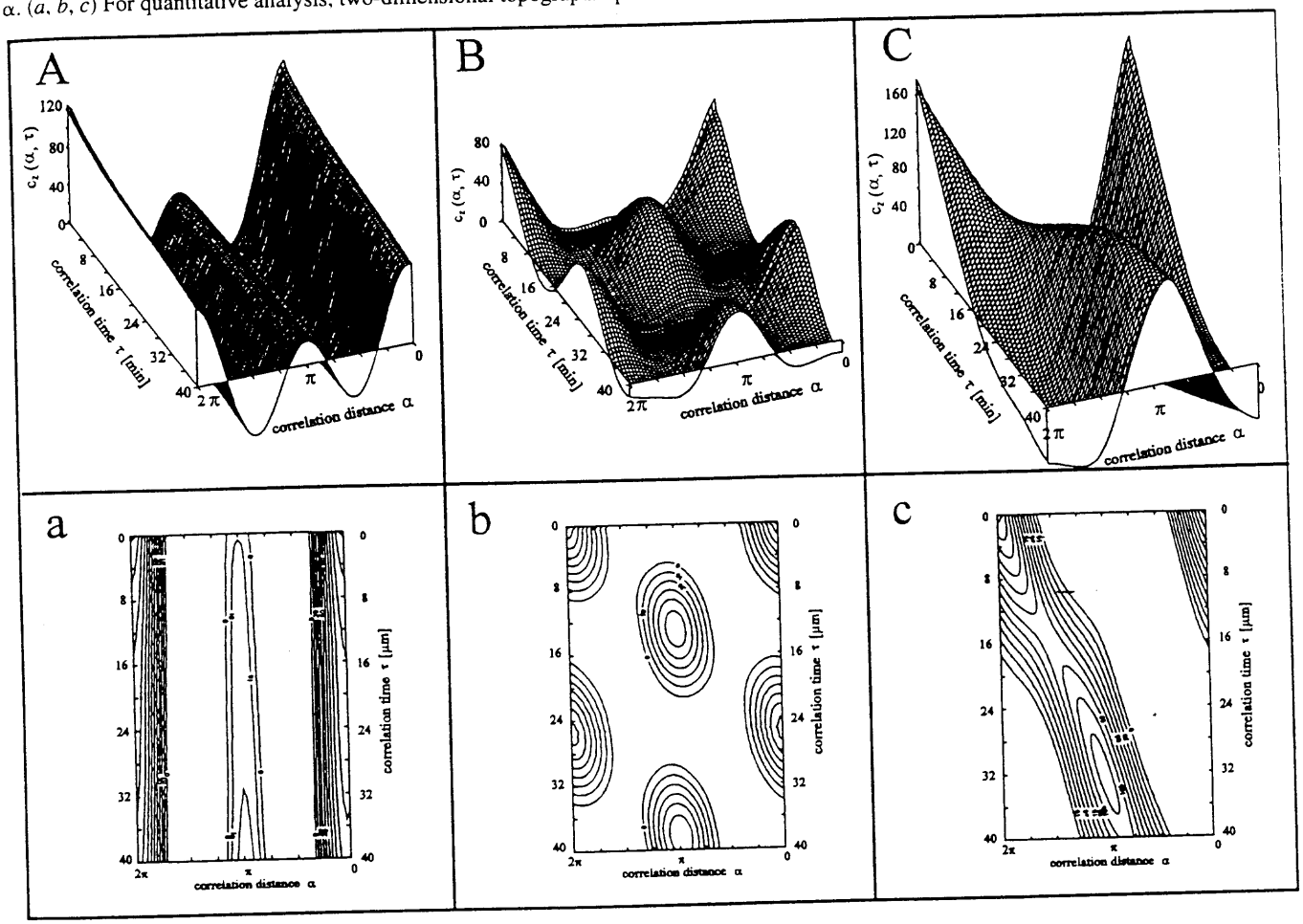

The dynamics of $L(\varphi, t)$ is finally determined by an analogus balance equation for the normal force components, mimicking the one-dimensional equations 7–10, but again regarding the additional surface tension (τ), with retractivity coefficient γ and constant protrusivity β resulting from intracellular hydrostatic pressure.

$$[13] \quad \partial_t L = \beta - \gamma L + \delta/a\partial_\varphi(\tau a \partial_\varphi L)$$

Equations 11–13 together result in a well-posed evolution equation system to be solved on the unit circle ($0 < \varphi < 2\pi$). We should remark that the hypotheses of both models are based on the "principle" of internal hydrostatic pressure within the cell body, clearly depending on the overall concentration of the cortical actin layer around the cell body, inducing farther extensions at those places where F-actin concentration is lower, and vice versa. Computer simulations of spatially discretized versions of these dynamical systems were run for slight perturbations of the constant states and for various choices of relevant cytomechanical parameters.

Results

Ruffle dynamics

Short-term analysis

Two-dimensional spatiotemporal diagrams (Fig. 3D) were used to characterize ruffle dynamics in connection with movements of the cell edge in one cell region. Fast lamellipodial extension of 0.8–1.7 µm is followed by slow retraction of the lamellar tip, until membrane ruffles separate from the cell edge and move centripetally over the cell surface with constant velocity, while a new protrusion cycle starts. At the separation point, ruffles are slightly broadening perpendicular to the cell edge (arrows in Fig. 3D, best seen for the ruffle at $t \sim$ 250 min). Between 50 and 100 ruffle velocity values per temperature were achieved from graphical analysis. Ruffle velocity increased approximately linearly between 24°C and 34°C and slowed down at 38°C. Results are shown in Fig. 5A combined with a linear regression over all values. In contrast with normal HEK, transfected keratinocytes (see Fig. 5) generally

showed a stronger temperature sensitivity and 60% of the cell population reacted with extensive blebbing at 38°C; the remaining 40% exhibited unexpectedly low activity. Observation of active cells revealed a pronounced periodicity in ruffle movement. In most cases, membrane ruffles were formed at regular frequencies and moved with corresponding velocity towards the cell body. To obtain general statements about ruffle periodicity, long-term recordings were analyzed.

Long-term analysis

Figure 6B shows the topographic line representation of the autocorrelation function calculated for the luminance profile of a typical HEK region with ruffling activity at 31°C (Fig. 6A). A region of high correlation is clearly seen in the surroundings of the reference point $\alpha = 0$, $\tau = 0$ and can be interpreted as a typical ruffle with x-extension, velocity, and time course representative for all observed ruffles. The typical ruffle exists for about 3 min and covers a distance of 5 μm in this time; it starts with a high velocity, decreasing after 25 s to a constant value. The ruffle slows down again about 20 s before complete disappearance. Two ridges of high correlation run parallel to the typical ruffle in an interval of 2.15 min in positive and negative correlation time, indicating a high periodicity of ruffle formation during the observation period. Although cells differ in frequency and velocity of appearing ruffles, strong periodicity of ruffle formation is typical for all analyzed HEK.

Dynamics of lamellipodia and filopodia

Lamellipodia arise with short acceleration, extend with constant speed, slow down, and retract with diminished velocity. Filopodia protrude from the very beginning with constant velocity and slow down eventually. In both cases, periods of constant extension were measured and resulted in 50 values per temperature. Relative distribution of the velocity values in Figs. 5B and 5C is equivalent to the course of ruffle velocity. Temperature dependence is linear between 26°C and 34°C, getting saturated including results at 38°C. The corresponding results of transfected keratinocytes are illustrated simultaneously. Temperature dependence of the speed of ruffles, lamellipodia, and filopodia was compared by calculating linear regression between 26°C and 34°C (Fig. 5D). One-dimensional filopodia are the first cell protrusions to reach new territory because of their high extension rates. They are followed by lamellipodia extending in two dimensions. In contrast with the fast outward extension of lamellipodia and filopodia, retracting lamellipodia and ruffles move inwards at slower rates.

Transfected cells seem to have a generally higher motility than normal cells. This hypothesis was tested using the F-test for equality of regression lines. For all three velocities (ruffles, lamellipodia, and filopodia), the regression lines depending on temperature differ significantly (Table 1). The question remains whether these differences are relevant on the background of a quite large intercellular variation as shown in Fig. 5. Therefore, we adjusted a mixed linear model for the velocity V_{ijkl} of ruffles, lamellipodia, and filopodia:

$$[14] \quad V_{ijkl} = \alpha_i + \beta_j + (\alpha\beta)_{ij} + \gamma_{ijk} + \epsilon_{ijkl}$$

where α_i is the fixed effect of cell type, β_j is the fixed effect of temperature, $(\alpha\beta)_{ij}$ is the fixed effect of interaction between cell type and temperature, γ_{ijk} is the random effect of individual cells, and ϵ_{ijkl} is the random error (Table 2). As expected, temperature and individuality of cells have a highly significant influence on mean velocity and its variation, respectively. Cell type has a highly significant influence on mean variation of velocity. Cell type has a highly significant influence on lamellipodial extension and is of borderline significance in velocity of ruffles and filopodia. We concluded that trHEK might be distinguished from nHEK by their higher motility and higher temperature sensitivity.

Fig. 10. Simulation of period protrusion and retraction of the lamella tip according to the one-dimensional model, equations 6–10. Plot of F-actin distribution $a(x, t)$ over a lamella section from the fixed position of the cell body ($x = 0$, left) to the movable tip ($x = L(t)$, right, where the a-plot drops to 0) for increasing time, $t = 0$ (back) up to $t = 2$ min (front), with averaged lamella length scaled to 1 (from Alt (1990), Fig. 3a). For a particular choice of parameters, the whole cycle of extension and retraction, lasting about 1.1 min, shows a steady increase of F-actin concentration at the lamella tip until, suddenly, a new protrusion with initially low F-actin concentration forms and extends, while a wave of locally condensed F-actin disrupts from the tip and moves back to the cell body, with a speed comparable with the preceding speed of tip retraction (about one lamella length per minute).

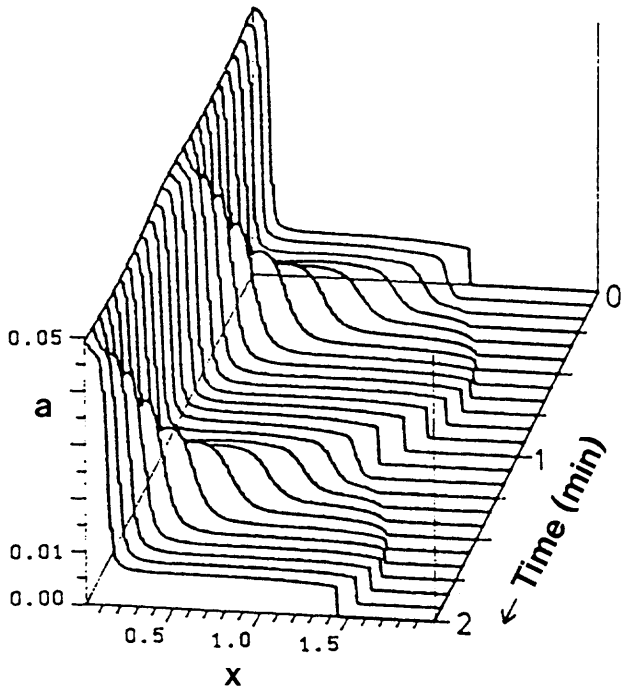

Two-dimensional analysis of lamellar dynamics

The sequence of phase-contrast images of a typical trHEK (Fig. 7A) in intervals of 24 min reveals an active cell with obvious formation and retraction of lamellae. It is remarkable that new lamellae emerge preferentially in regions where lamellae extended and retracted before (here at 0, $2/3\pi$, and $4/3\pi$ on the cell periphery, see arrowheads in Fig. 7B). The normal extension of the cell outline from the momental ellipse,

Fig. 11. Simulation of peripheral protrusion dynamics according to the circular model, equations 11–13. Topographic plot of protrusion length $L(\varphi, t)$ in a φ–t diagram analogous to Fig. 8. (A) For a certain range of cytomechanical parameters ($a = 1$, $\eta = 0.5$, $\beta = \gamma = 0.15$, $\delta = 0.025$, $\tau = 7$, $\mu = 1$, $\psi = 10$, and $\sigma_0 = 0.1$), we obtain, after a short initial transient period, a regularly alternating pulsation of two opposite lamellae with a period of about 35 min, compared with an assumed mean F-actin assembly time of 2 min. However, after the first pulsation cycle, the lamellar protrusions already show a tendency to rotate in a counterclockwise direction with a speed that runs half around the (circular model) cell in half the cycle time. (B) For slightly changed parameters, with relaxed contractivity and cortical surface tension, a rotating wave of one broad protrusion builds up spontaneously and finally attains a constant speed with one rotation in about 25 min. The shape of the lamella wave is steeper in the front than in the back (visualized by taking a cross section through the contour lines for fixed time, t) and shows a weak pulsation of broadening and shrinking with a period of about 15 min.

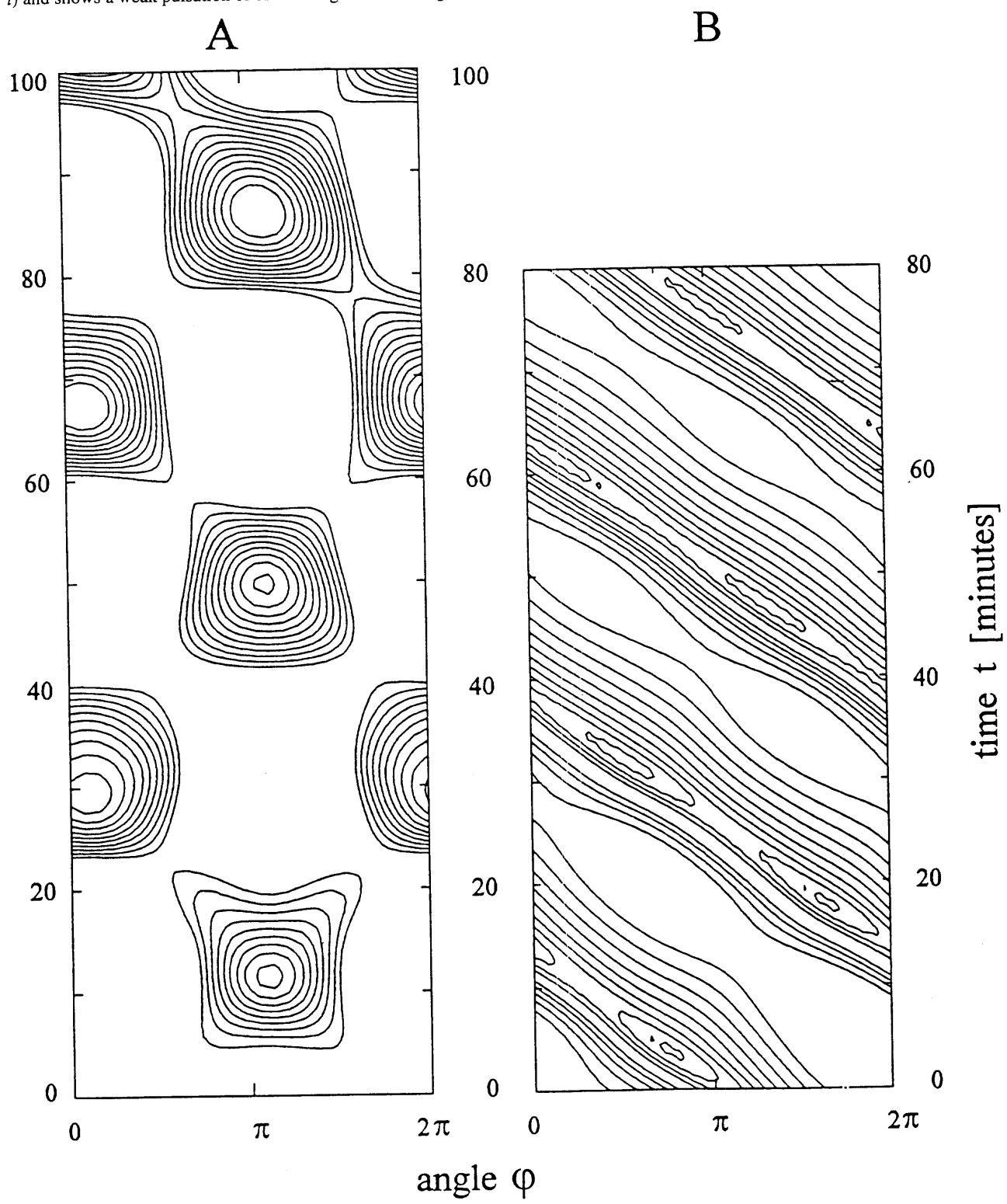

which approximates the cell body, is a good measure for the lamellar protrusion and was evaluated in topographical plots. Figure 8A shows the topographic line plot of an nHEK with typical behaviour observed over a period of 200 min. Only topographic lines above the expectation value were plotted. Lamellae are alternating in two antipodal regions of the cell ($\pi/2$ and $3/2\pi$). Formation of a new lamella (at $\pi/2$, 100 min) lasts for about 40 min accompanied by reduction in extension and subsequent retraction of the antipodal lamella.

All 30 observed cells, including trHEK, showed succession of lamellae in two or three outstanding regions of the cell periphery but revealed differences in persistence time of lamellae as well as in duration of lamella extension dependent on lamella retraction in another region. Lamellae of all 15 trHEK generally alternated with higher frequencies than was seen on nHEK. Two observed trHEK (trHEK-1 and trHEK-2) had a remarkably regular behaviour. trHEK-1 (Fig. 8B) extended antipodal lamellae at $\pi/4$ and $5/4\pi$, alternating periodically with high frequency (persistence time, 10 min; duration of a cycle, 25 min). There was almost no simultaneous coexistence of these two lamellae. A small difference between the two lamellar regions may be distinguished: lamellae at $\pi/4$ shifted their location constantly from $\pi/4$ to 0 at the cell periphery during their 10-min existence, whereas the lamellae at $5/4\pi$ remained stable on average. trHEK-2 (Fig. 8C) showed no alternating formation of lamellae at different regions but exhibited a persistent lamella during the whole observation period of 200 min rotating counterclockwise with constant velocity of 65 min per turn around the cell periphery. While the leading front of the lamella remained stable, extension of the lamella increased and decreased regularly over time. Even in this case, two preferred regions of maximal extension were detectable at π and 2π.

A quantification of the pattern of lamellar dynamics was obtained by calculating the spatiotemporal autocorrelation of the cell outline. Autocorrelation of the typical nHEK (Fig. 9A) showed that the lamellae have a mean width of 3/8 cell circumference (width of the ridge at $\alpha = 0$ and $\tau = 0$ is $3/4\pi$) and a mean persistence time of more than 40 min (autocorrelation at $\alpha = 0$ decreases slowly and is still high at $\tau = 40$). There were periods with two simultaneous antipodal lamellae, as indicated by the ridge at $\alpha = \pi$: increasing autocorrelation values for increasing correlation time τ (Fig. 9*a*) mean that formation of a new lamella is correlated to a retraction of the antipodal one.

trHEK-1 had an autocorrelation pattern of high regularity (Fig. 9B), representing two alternating antipodal lamellae (peaks of the autocorrelation function alternating at $\alpha = 0$ and $\alpha = \pi$) during the whole observation interval. Lamella had a mean width of 3/8 cell circumference (width of the ridge at $\alpha = 0$ and $\tau = 0$ is $3/8\pi$), a persistence time of 10 min (decrease to 0 at $\alpha = 0$ in a correlation time $\tau = 10$ min), and a period of about 25 min indicated by the second maximum at $\alpha = 0$ and $\tau = 25$ min (Fig. 9*b*). On the average, lamellae showed a change in location of 1/16 cell circumference per 10 min. There were no overlap time periods of antipodal lamellae.

The autocorrelation peak of trHEK-2 (Fig. 9C) moved with increasing time distance from $\alpha = 0$ to $\alpha = \pi$ after 32 min. This points to a lamellar wave rotating around the cell periphery with a constant averaged velocity. Width and outward extension of the lamella increased and decreased with a period of 32 min, as shown by minimal height and maximal width of the autocorrelation ridge at $\alpha = 3\pi/2$ and $\tau = 16$ min, and vice versa (maximal height and minimal width) at $\alpha = \pi$ and $\tau = 32$ (Fig. 9*c*).

Almost all analyzed HEK showed similar behaviour. Cells have two or three preferred regions of lamellae formation lying at maximal distance (π for two lamellae, $2/3\pi$ for three lamellae). In most cases, lamellae formation alternates, with a new protrusion starting only if the previous one is retracting. Most lamellae repeatedly occur at the same location, and even cell trHEK-2, with a rotating lamellar front, had tow antipodal regions where the passing wave attained a broader shape.

Comparison with cytomechanical model simulations

The more or less regular cycle of protrusion and retraction of the lamellar tip with accompanying centripetal waves of ruffles along a one-dimensional section line (Fig. 3D) suggests looking for periodic solutions of the one-dimensional lamellar model equations 6–10. Indeed, for a wide range of cytomechanical parameters that reduce the effective mechanochemical assembly rate for low F-actin concentration by local swelling of the meshwork but induce its rapid contraction for moderately higher concentrations, we obtain (Fig. 10) a regular protrusion–retraction cycle with a period of 1 min for an assumed chemical assembly rate $\eta = 0.5\ \text{min}^{-1}$, but we get a period of 2 min for $\eta = 0.25\ \text{min}^{-1}$, comparing well with the averaged period of 2.15 min evaluated from long-term analysis (Fig. 6). Also, when looking at Fig. 3C from downside and reversing the time axis so that valleys (of darker luminance) become ridges, two repetitive cycles would resemble the simulated picture in Fig. 10. Moreover, the model simulations reproduce the observed cycle of continuing F-actin assembly in a newly expanding lamellar tip, which later induces its retraction and, finally, forms a retrograde wave of concentrated actin network, comparable with a ruffle, whose width and speed decrease as it approaches the border of the cell body ($x = 0$). Already on its way, namely for values $a > a_* = 0.01$, disassembly of F-actin takes over until F-actin concentration reaches its mechanochemical equilibrium value for $a = 0.05$ at the cell body, where it forms a steady contracted network.

The two-dimensional shape deformation model described by the system of equations 11–13 is even more crude than the one-dimensional model; nevertheless, it also reproduced several typical features of the observed dynamical patterns illustrated in Fig. 8. Indeed, the cytomechanical parameters can be chosen so that steady lamellar protrusions or alternating pulsations or rotating waves of any given mode number are simulated (counting the number of lamellar protrusions around the cell periphery) (compare with Alt and Tranquillo 1995). Here we only present two nearly related cases with mode number 1, namely a pulsating pattern of period 35 min (Fig. 11A) and a rotating wave pattern of period 25 min (Fig. 11B). In the topographic plot (A), the first single lamella shows a tendency to split at the end, around $t = 20$ min, a property that may also be recognized in the right lamella of Fig. 8B. The left lamella, and also the right one after $t = 120$ min, has an increasing tendency to move to the left: a similar effect is clearly seen in the simulation picture (Fig. 11A) for $t \geq 50$ min, finally leading to a pulsating rotation wave. For the slightly changed parameters in plot B, such as wave appears much earlier and with a shorter period of 25 min. Notice that by further slowing down the time rates, by a factor of 2.5, the period would enlarge by this factor, comparing well with the period of about 65 min seen in

Fig. 8C. Also, the lamellar protrusion wave is steeper at the front and shows (irregular) pulsations in width of a period of about 35 min, which is in the same relative range as the corresponding 15-min pulsations in Fig. 11B.

Certainly, the analogy between observed and simulated protrusion patterns can be made only on the average, as stochastic perturbations are not considered in the mathematical model (Tranquillo and Alt 1995) and, in principle, as the assumed biochemical and cytomechanical hypotheses for the cortical actin model are held very simple: first-order (dis)assembly kinetics, linear influence of cortical surface tension and curvature, and idealization of the actomyosin network as a contractile, highly viscous reactive fluid (Dembo 1989). Nonetheless, the most important features of protrusion dynamics are captured.

Discussion

Although stimulation of nHEK motility and locomotion by external chemical factors such as EGF or by changes of the extracellular matrix seems to be the rule for processes as regeneration and wound healing in vivo, the distinguished motile and proliferative behaviour of trHEK is probably due to abnormalities in the internal regulation of cell–cell or cell–substrate adhesions or of motility forces. Thus, it makes sense to study patterns of spontaneous motility of single adherent HEK in vitro by phase-contrast video microscopy to reveal the underlying cytomechanical properties by consistent analysis and interpretation of image sequences. For our project, we did not perform direct or indirect measurement of forces, on-line immunofluorescent staining, or other estimations of F-actin mass distribution (compare with Dunn and Brown 1990 or Bereiter-Hahn and Lüers 1994). In spite of the better contrast of cell outlines or ruffles, we did not evaluate differential-interference contrast (DIC) video images because these contours appear to vanish at certain directional angles of the view field.

Therefore, we tried to handle digitized luminance (inverse grey level) data of images, as in Figs. 3A or 7A, by suitable edge detection algorithms. Surprisingly, the analysis of data along section lines transversal to the cell edge revealed a common periodicity and correlation in the protrusion–retraction pattern of lamellae and ruffles or all treated cells. Lamellipodial protrusion is relatively fast (2–6 μm/min for normal HEK, even faster for transfected HEK) but is still only half the speed of filopodial extension (4–9 μm/min). Retraction of a lamella is much slower (1–4 μm/min), occurring, at the same speed as ruffles, which appear near the tip and disrupt from it in the moment of new lamellipod extension (Fig. 3D). These events occur repeatedly with a period of about 2 min (Fig. 6). Interestingly, similar phenomena of repeated waves of disruption and centripetal movement of concentrated F-actin sheets were observed in amoeboid cells as Chaos carolinensis (Grebeçki 1990) or even in cytoplasma extracts from Xenopus oocytes (Ezzell et al. 1983) with the only difference being that their frequency and speed is much higher (about 0.5 and 5 μm/s, respectively). Nevertheless, the striking analogy suggests a common mechanism for such a universal cytomechanical phenomenon with the only difference being scaling in different geometric situations or physiological conditions.

We have presented one possible cytomechanical model that yields consistent simulation patterns (Fig. 10), with regular cycles of tip protrusion and retraction as well as disruption of ruffle waves with a speed (one lamella length, about 3–5 μm/min), comparing well with the observed one. We also notice striking similarity to measurements of retrograde F-actin transport in nerve growth cones, 3–8 μm/min (Forscher and Smith 1988), and in fibroblasts, 4.5 × 0.3 μm/min (Symons and Mitchison 1991), whereas the faster F-actin mediated transport of particles in fish keratocytes, about 20 μm/min (Kucik et al. 1990), seems to be correlated with a comparably faster cell migration. In our study of spontaneous motility, the position of keratinocytes is mostly stationary. Correspondingly, the theory predicts a steady cycle of F-actin assembly at the tip, of cortical flow towards the cell body, and of disassembly at the cell body (compare Dembo et al. 1984, Alt 1987, or Bray and White 1988). In the simulations (Fig. 10), speed of centripetal F-actin transport stays quite constant over the lamella and decreases only near the cell body, consistent with the observed speed behavior of ruffles (Fig. 6). Forscher and Smith (1988) have argued that such a uniform speed contradicts the hypothesis of (myosin-II mediated) network contraction, but in our model, contraction preferentially happens at higher F-actin concentrations, i.e., only near the cell body. This local contractile force is propagated into the highly viscous actin meshwork in the lamella and induces the retrograde transport, while gradually depleted regions near the tip are continuously filled by reassembling or polmerizing filaments.

The model works in spite of the simplifying assumption that ATP, G-actin, and all relevant actin-binding proteins (myosin II, gelsolin, filamin, etc.) are homogeneously distributed at sufficient concentrations. The essential feature is that assembly or disassembly, contraction or swelling, and also membrane interactions of the F-actin network are regulated just by its concentration. Moreover, only concentration and velocity of the network regulate the hydrostatic pressure drop between cell body and tip. Although other mathematical models consider much more detailed molecular regulation processes (Oster and Perelson 1987; Skierczynski et al. 1994), they are not yet able to reproduce the observed universal dynamics of lamellae and ruffles. However, we notice that swelling pressure in our model has similar effects as osmotic pressure or thermodynamic fluctuations of the plasma membrane in other models (Peskin et al. 1993). Finally, by taking into consideration kinetics and transport of regulatory proteins throughout the lamella or interaction of actin filaments with transmembraneous adhesion proteins, we could generalize the model equations without altering the basic lamellar dynamics but allowing a more detailed quantitative fit of the observed motility patterns and their spatiotemporal correlations.

Similar arguments hold for possible explanations of the observed circular protrusion patterns and their angular-temporal correlations (Figs. 8 and 9). These are regularly alternating pulsations of extension and retraction (with a period of 25 min) as well as extension waves rotating around the cell periphery (with a remarkably constant wave speed of one circulation per hour). Similar patterns have been observed and analyzed with Dictyostelium discoideum cells by Killich et al. (1993). Moreover, periodicities in leading lamellar protrusions of migrating cells can induce periodic alteration in velocity and direction of paths as shown in the analysis of leukocyte locomotion by Murray et al. (1992), Brosteanu (1994), and Hartmann et al. (1994).

Attempts have been made to explain the coordinated peripheral cell extensions and retractions by local activation, e.g., Ca^{2+} mediated, near a protrusion with simultaneous inhibition at the surrounding regions of the cell periphery (Meinhardt 1982, p. 44 ff; Killich et al. 1994). In contrast, our cytomechanical setup again neglects all eventual regulatory effects of diffusing substances as Ca^{2+} or Profilin, and yet it is able to reproduce the observed patterns of cell shape deformations in principle (Fig. 11). Although details of time course and shape geometry of lamellar motility are not within the scope of our simple circular cortex model, we claim, supported by the presented simulations, that the basic universal mechanisms for lateral coordination of lamellipodial protrusion are the following two globally effective physical properties of the dynamic cortical cytoskeleton: (*i*) local regulation of hydrostatic pressure at the plasma membrane by induction of intralamellar drag forces and tension in the cortical surface, and (*ii*) local stabilization or weakening of the cortical actin network by viscocontractile tensions and assembly–disassembly. This view is consistent with the observed alternations in F-actin structure around the cell cortex: dense bundles of so-called stress fibers in stretched regions without lamellae and dispersed distribution behind regions of lamellar protrusions. Further image and correlation analysis of video micrographs as well as more detailed cytomechanical modeling should be performed to study the effects that are due to deformation of the cell body, to variations in length and orientation of actin filaments, and finally to cell–substrate adhesion.

Acknowledgements

Transfected keratinocytes (trHEK) were kindly provided by the laboratory of Edward O'Keefe (Department of Dermatology, University of North Carolina). Other laboratory facilities were available at the Department of Dermatology, University Bonn. O. Brosteanu and B. Hinz were supported by a VW grant on "Cooperative cell movement" (1992–1995), which also provided video microscopy and image-processing equipment. Furthermore, we gratefully acknowledge the assistance of Werner Heiße (Division of Theoretical Biology, University Bonn), who developed and implemented a program for automatic cell edge detection.

References

Abercrombie, M., Heaysman, J.E.M., and Pegrum, S.M. 1970. The locomotion of fibroblasts in culture. II. "Ruffling." Exp. Cell Res. **60**: 437–444.

Alt, W. 1987. Mathematical models in actin–myosin interaction. Progr. Zool. **34**: 219–229.

Alt, W. 1990. Mathematical models and analysing methods for the lamellipodial activity of leukocytes. NATO ASI (Adv. Sci. Inst.), Ser. H, Cell Biol. **42**: 407–422.

Alt, W., and Kaiser, H.W. 1994. Observation, modeling and simulation of keratinocyte movement. NATO ASI (Adv. Sci. Inst.), Ser. H, Cell Biol. **84**: 445–451.

Alt, W., and Tranquillo, R.T. 1995. Basic morphogenetic system modeling shape changes of migrating cells: how to explain fluctuating lamellipodial dynamics. *In* Proc. 2nd European conference in mathematics applied in biology and medicine. Lyon, Dec. 1993. World Scientific, Toronto, Ont.

Barbosa, M.S., and Schlegel, R. 1989. The E6 and E7 genes of HPV-18 are sufficient for inducing two-stage in vitro transformation of human keratinocytes. Oncogene, **4**: 1529–1532.

Bereiter-Hahn, J., and Lüers, H. 1994. The role of elasticity in the motile behaviour of cells. NATO ASI (Adv. Sci. Inst.), Ser. H, Cell Biol. **84**: 181–230.

Bray, D., and White, J.G. 1988. Cortical flow in animal cells. Science (Washington, D.C.), **239**: 883–888.

Bray, D., Money, N., Harold, F., and Bamburg, J. 1991. Responses of growth cones to changes in osmolarity of the surrounding medium. J. Cell Sci. **98**: 507–515.

Brosteanu, O. 1994. Methoden zur Analyse der Lamellipodienaktivität von Leukozyten. Dissertation, University of Bonn, Bonn, Germany.

Condeelis, J. 1993. Life at the leading edge: the formation of cell protrusions. Annu. Rev. Cell Biol. **9**: 411–444.

Condeelis, J., Bresnick, M.D., Dharmawardhane, S., Eddy, R., Hall, A.L. Sauterer, R., and Warren, V. 1990. Mechanics of amoeboid chemotaxis: an evaluation of the cortical expansion model. Dev. Genet. **11**: 333–340.

Cooper, J.A. 1991. The role of actin polymerisation in cell motility. Annu. Rev. Physiol. **53**: 585–605.

De Brabander, M., Nuydens, R., and Geerts, H. 1990. Dynamic cytomatrix–membrane interactions in cell shape and organization. NATO ASI (Adv. Sci. Inst.), Ser. H, Cell Biol. **42**: 215–234.

Dembo, M. 1989. Field theories of the cytoplasm. Comments Theor. Biol. **1**: 159–177.

Dembo, M., and Harris, A.K. 1981. The motion of particles adhering to the leading lamella of crawling cells. J. Cell Biol. **91**: 528–536.

Dembo, M., Harlow, F.H., and Alt, W. 1984. The biophysics of cell surface mobility. *In* Cell surface dynamics, concepts and models. *Edited by* A.E. Perelson, Ch. DeLisi, and F.W. Wiegel. Marcel Dekker, N.Y., Basel. pp. 495–542.

Donaldson, D.J., and Mahan, J.T. 1988. Keratinocyte migration and the extracellular matrix. J. Invest. Dermatol. **90**: 623–627.

Dunn, G.A., and Brown, A.F. 1990. Quantifying cellular shape using moment invariants. Lect. Notes Biomath. **89**: 10–34.

Evans, E. 1993. New physical concepts for cell amoeboid motion. Biophys. J. **64**: 1306–1322.

Ezzell, R.M., Brothers, A.J., and Cande, W.Z. 1983. Phosphorylation-dependent contraction of actomyosin gels from amphibian eggs. Nature (London), **306**: 620–623.

Fath, K.R., and Burgess, D.R. 1994. Membrane motility mediated by unconventional myosin. Curr. Opin. Cell Biol. **6**: 131–135.

Felder, S., and Elson, E.L. 1990. Mechanics of fibroblast locomotion: quantitative analysis of forces and motion at the leading lamellas of fibroblasts. J. Cell Biol. **111**: 2513–2526.

Fisher, G., Conrad, P.A., DeBasio, R.L., and Taylor, R.B. 1988. Centripetal transport of cytoplasm, actin, and the cell surface in lamellipodia of fibroblast. Cell Motil. Cytoskeleton, **11**: 235–247.

Forscher, P., and Smith, S.J. 1988. Actions of cytochalasins on the organisation of actin filaments and microtubules in neuronal growth cone. J. Cell Biol. **107**: 1505–1516.

Giuliano, K.A., and Taylor, D.L. 1994. Fluorescent actin analogs with a high affinity for profilin in vitro exhibit an enhanced gradient of assembly in living cells. J. Cell Biol. **124**: 971–983.

Giuliano, K.A., and Taylor, D.L. 1995. Measurement and manipulation of cytoskeletal dynamics in living cells. Curr. Opin. Cell Biol. **7**: 4–12.

Grebeçki. A. 1990. Dynamics of the contractile system in pseudopodial tips of normally locomoting amoebae, demonstrated in vivo by video-enhancement. Protoplasma, **54**: 98–111.

Grebeçki, A. 1994. Membrane and cytoskeletal flow in motile cells with emphasis on the contribution of free living amoebae. Int. Rev. Cytol. **148**: 37–80.

Green, H., Kehinde, O., and Thomas, J. 1979. Growth of cultured human epidermal cells into multiple epithelia suitable for grafting. Proc. Natl. Acad. Sci. U.S.A. **76**: 5665–5670.

Harris, A.K., and Dunn, G.A. 1972. Centrifugal transport of attached particles on both surfaces of moving fibroblasts. Exp. Cell Res. **73**: 519–523.

Harris, A.K., Wild, P., and Stopak, D. 1980. Silicone rubber substrata: a new wrinkle in the study of cell locomotion. Science (Washington, D.C.), **208**: 177–179.

Hartmann, R.S., Lau, K., Chou, W., and Coates, T.D. 1994. The fundamental motor of the human neutrophil is not random: evidence for the local non-Markov movement in neutrophils. Biophys. J.

Hartwig, J.H. 1992. Mechanisms of actin rearrangements mediating platelet activation. J. Cell Biol. **118**: 1421–1442.

Hartwig, J., and Kwiatkowski, D. 1991. Actin binding proteins. Curr. Opin. Cell Biol. **3**: 87–97.

Heath, J.P., and Holifield, B.F. 1991. Cell locomotion: new research tests old ideas of membrane and cytoskeletal flow. Cell Motil. Cytoskeleton, **18**: 245–257.

Killich, T., Plath, P.J., Xiang, W., Bultmann, H., Rensing, L., and Vicker, M.G. 1993. The locomotion, shape and pseudopodial dynamics of unstimulated Dictyostelium cells are not random. J. Cell Sci. **106**: 659–667.

Killich, T., Plath, P.J., Haß, E.-C., Xiang, W., Bultmann, H., Rensing, L., and Vicker, M.G. 1994. Cell movement and shape are non-random and determined by intracellular, oscillatory rotating waves in Dictyostelium amoebae. BioSystems, **33**: 75–87.

Kolega, J. 1986. Effects of mechanical tension on protrusive activity and microfilament and intermediate filament organisation in an epidermal epithelium moving in culture. J. Cell Biol. **102**: 1400–1411.

Korohoda, W., Vöth, M., and Bereiter-Hahn, J. 1992. Biphasic response of human polymorphonuclear leucocytes and keratinocytes (epitheliocytes) from Xenopus *laevis* to mechanical stimulation. Protoplasma, **167**: 169–174.

Kucik, D.F., Elson, E.L., and Sheetz, M.P. 1990. Cell migration does not produce membrane flow. J. Cell Biol. **111**: 1617–1622.

Lee, J., Ishihara, A., Theriot, J.A., and Jacobson, K. 1993. Principles of locomotion for simple-shaped cells. Nature (London), **362**: 167–171.

Lee, J., Leonard, M., Oliver, T., Ishihara, A., and Jacobson, K. 1994. Traction forces generated by locomoting keratocytes. J. Cell Biol. **127**: 1957–1964.

Luby-Phelps, K. 1994. Physical properties of cytoplasm. Curr. Opin. Cell Biol. **6**: 3–9.

Meinhardt, H. 1982. Models of biological pattern formation. Academic Press, London.

Murray, J. Vawter-Hugart, H., Voss, E., and Soll, D.R. 1992. Three-dimensional motility cycle in leucocytes. Cell Motil. Cytoskeleton, **22**: 211–223.

Nachmias, V.T. 1993. Small actin-binding proteins: the ß-thymosin family. Curr. Opin. Cell Biol. **5**: 56–62.

Oster, G. 1984. On the crawling of animal cells. J. Embryol. Exp. Morphol. **83**: 329–364.

Oster, G., and Perelson, A. 1987. The physics of cell motility. J. Cell Sci. **8**: 35–54.

Oster, G., Perelson, A., and Tilney, L. 1982. A mechanical model for elongation of the acrosomal process in Thyone sperm. J. Math. Biol. **15**: 259–265.

Peskin, C., Odell, G., and Oster, G. 1993. Cellular motion and thermal fluctuations: the brownian ratchet. Biophys. J. **65**: 316–324.

Pring, M., Weber, A., and Bubb, M.R. 1992. Profilin–actin complexes directly elongate actin filaments at the barbed end. Biochemistry, **31**: 1827–1836.

Rheinwald, J.G. 1975. Serial cultivation of strains of human epidermal keratinocytes: the formation of keratinizing colonies from single cells. Cell, **6**: 331–336.

Schmidt, C.E., Horwitz, A.F., Lauffenburger, D.A., and Sheetz, M.P. 1993. Integrin–cytoskeletal interactions in migrating fibroblasts are dynamic, asymmetric, and regulated. J. Cell Biol. **123**: 977–991.

Sheetz, M.P., Wayne, D.B., and Pearlman, A.L. 1992. Extension of filopodia by motor-dependent actin assembly. Cell Motil. Cytoskeleton, **22**: 160–169.

Skierczynski, B.A., Usami, S., and Skalak, R. 1994. A model of the leukocyte migration through solid tissue. NATO ASI (Adv. Sci. Inst.), Ser. H, Cell Biol. **84**: 285–328.

Stossel, T.P. 1993. On the crawling of animal cells. Science (Washington, D.C.), **260**: 1086–1094.

Symons, M.H., and Mitchison, T.J. 1991. Control of actin polymerisation in live and permeabilized fibroblasts. J. Cell Biol. **114**: 503–513.

Theriot, J.A., and Mitchison, T.J. 1991. Actin microfilament dynamics in locomoting cells. Nature (London), **352**: 126–131.

Tranquillo, R.T., and Alt, W. 1995. Stochastic model of receptor-mediated cytomechanics and dynamic morphology of leukocytes. J. Math. Biol. In press.

Vasiliev, J.M. 1991. Polarisation of pseudopodial activities: cytoskeletal mechanisms. J. Cell Sci. **98**: 1–4.

Wang, Y.-L. 1985. Exchange of actin-subunits at the leading edge of living fibroblasts: possible role of treadmilling. J. Cell Biol. **101**: 597–602.

Weeds, A., and Maciver, S. 1993. F-actin capping proteins. Curr. Opin. Cell Biol., **5**: 63–69.

Zigmond, S. 1993. Recent quantitative studies of actin filament turnover during cell locomotion. Cell Motil. Cytoskeleton, **25**: 309–316.